CHALMERS
UNIVERSITY OF TECHNOLOGY

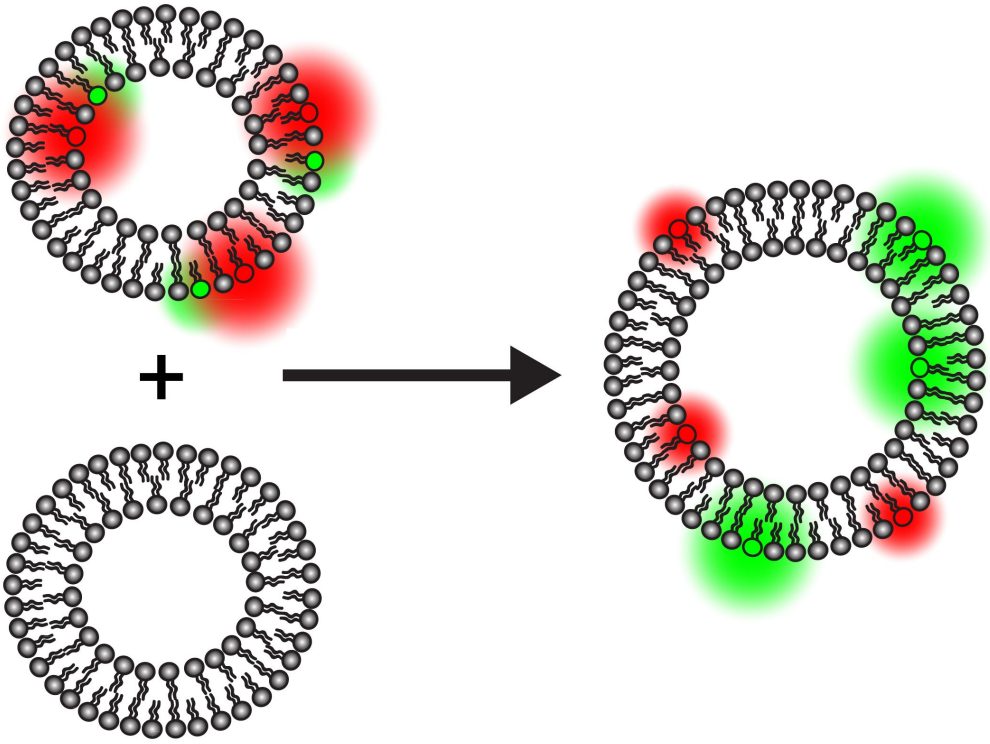

A FRET based assay for the quantification of synthetic and native lipid vesicles

Master's thesis in Applied Physics

KONRAD THORSTEINSSON

Department of Physics
CHALMERS UNIVERSITY OF TECHNOLOGY
Gothenburg, Sweden 2018

Master's thesis 2018

A FRET based assay for the quantification of synthetic and native lipid vesicles

KONRAD THORSTEINSSON

CHALMERS
UNIVERSITY OF TECHNOLOGY

Department of Physics
Division of Biological Physics
Chalmers University of Technology
Gothenburg, Sweden 2018

A FRET based assay for the quantification of synthetic and native lipid vesicles
KONRAD THORSTEINSSON

Supervisor: Marta Bally, Department of Clinical Microbiology, Umeå University
Examiner: Julie Gold, Department of Physics

Master's Thesis 2018
Department of Physics
Division of Biological Physics
Chalmers University of Technology
SE-412 96 Gothenburg
Telephone +46 31 772 1000

Cover: FRET labelled lipid vesicle fusing with an unlabelled lipid vesicle. Adapted with permission from Pace *et al* (2015).

Typeset in LaTeX
Printed by Chalmers Digital Print
Gothenburg, Sweden 2018

A FRET based assay for the quantification of synthetic and native lipid vesicles
KONRAD THORSTEINSSON
Department of Physics
Chalmers University of Technology

Abstract

Lipid nanoparticles, both of artificial and biological origin, have attracted significant attention in recent years. Biological lipid nanoparticles in the form of extracellular vesicles are involved in intercellular communication and biological material transport. Synthetic liposomes have also been proposed as promising drug delivery systems. In view of this broad interest, methods capable of accurately quantifying the content of lipid nanoparticles in a sample are urgently needed. To date, quantification is most commonly achieved by counting the particles after visualization, or by quantifying the total protein content in the case of particles of biological origin.
In this thesis we present an alternative method allowing for the quantification of the total lipid surface area of an unknown sample. Our approach is based on Förster Resonance Energy Transfer (FRET), where the unknown lipid nanoparticle sample is sonicated with vesicles containing a FRET-fluorophore pair, leading to membrane fusion. The change in FRET fluorescence can then be correlated to the total surface area of the unknown sample. We first calibrated the method using synthetic vesicles of known surface area. We then tested the method on synthetic vesicles containing cholesterol, herpes simplex virus type 2, and two species of outer membrane vesicles secreted from *E. coli* bacteria. Finally, we benchmarked our results against alternative established methods and discussed potential and limitation of each.
Our results indicate that the FRET assay is suitable to quantify all the lipid nanoparticle samples tested here and serves as a viable measurement technique to quantify lipid surface areas.

Keywords: FRET, membrane fusion, surface area, liposomes, vesicles, NTA, *E. coli*, HSV-2.

Acknowledgements

I would like to thank Marta Bally, my thesis supervisor, for giving me the opportunity to do this project, and for all the assistance and teaching she has provided me with for its duration. Hudson Pace at the Department of Integrative Medical Biology, Umeå University, who developed this project and offered substantial insight into its development. And Julie Gold at the Department of Physics, Chalmers, the thesis examiner, for all the assistance and feedback she has provided.
I would also like to thank the many people who helped with various aspects of the project itself. At the Biological Physics Division at the Department of Physics, Chalmers, I would like to thank Eneas Schmidt and Karin Norling for helping me perform measurements and teaching me methods required for the project. Eva Delin at Clinical Microbiology, Umeå University, who taught helped me with the spectrofluorometer and NTA. And Nils Skoglund at the Department of Applied Physics and Electronics at Umeå University, for his help and patience in assisting with the phosphorus assay.
Last but not least, I would like to thank Madeleine Ramstedt at the Department of Chemistry, Umeå University, and Thomas Bergström at the Department of Infectious Diseases, University of Gothenburg, for providing us with the biological samples used in this project (OMV and virus samples respectively).

Konrad Thorsteinsson, Gothenburg, November 2018

Contents

List of Acronyms

EV ..... **e**xtracellular **v**esicle
HBS ..... **H**EPES **b**uffered **s**aline
HSV-2 ..... **h**erpes **s**imples **v**irus - type **2**
NTA ..... **n**anoparticle **t**racking **a**nalysis
OMV ..... **o**uter **m**embrane **v**esicle
PBS ..... **p**hosphate **b**uffered **s**aline
SAC ..... **s**urface **a**rea **c**oncentration
TEM ..... **t**ransmission **e**lectron **m**icroscopy

List of Chemical Acronyms

CBQCA ..... 3-(4-**c**arboxy**b**enzoyl)**q**uinoline-2-**c**arbox**a**ldehyde
DHPE 1-2-**di****h**exadecanoyl-sn-glycero-3-**p**hospho**e**thanolamine
HEPES ..... 4-(2-**h**ydroxy**e**thyl)-1-**p**iperazine**e**thane**s**ulfonic acid
NBD 7-**ni**tro-2-1 3-**b**enzoxa**di**azol-4-yl
PE 1 2-dioleoyl-sn-glycero-3-**p**hospho**e**thanolamine
POPC 1-**p**almitoyl-2-**o**leoyl-SN-glycero-3-**p**hospho**c**holine

List of Figures

List of Tables

1
Introduction

1.1 Motivation

In recent years, the study of small lipid-bilayer enveloped structures (sometimes referred to as lipid nanoparticles or lipid vesicles[1]) has attracted significant amount of interest. For example, liposomes, artificially produced lipid vesicles, have been proposed as promising candidates as carriers for drug delivery applications. Another example of lipid nanoparticles of high relevance in biology and in biomedical applications are cell-secreted **e**xtracellular **v**esicles (**EV**s), which have been shown to be involved in a variety of biological processes, such as intercellular communication, disease propagation and inflammation reaction[2,3].

Currently, a variety of methods are used to characterize lipid nanoparticles in terms of size, shape, size distribution and molar concentrations. These methods include **t**ransmission **e**lectron **m**icroscopy (**TEM**) to measure size and structure[2–4], **n**anoparticle **t**racking **a**nalysis (**NTA**) to measure size, size distribution and concentration[2–5] and flow cytometry to measure size[2]. Each method has its advantages and disadvantages[2]. For instance, TEM requires the vesicles to be fixated and measured under vacuum, leading to changes in their size and shape[2], and NTA may give inaccurate results due to the large size distribution and low refractive index of EV's[2]. Different measurement principles may also lead to different measured values for the same property[4,6], further complicating measurements and comparisons across different studies[6]. For these reasons, research involving lipid nanoparticles are reliant on multiple measurement methods to give an adequate characterization of lipid nanoparticle systems. While the amount of material present in a lipid nanoparticle sample has most often been estimated either by counting particles using NTA[2,3,5] or by determining the total protein content[2], a complementary method to characterize lipid nanoparticle samples would be to quantify the total surface area of lipid membrane in a given sample. The development, implementation, and validation of such a method is at the center of this master's thesis project.

1.2 Theoretical background

1.2.1 Phospholipids and lipid structures

Phospholipids are amphiphilic molecules composed of two hydrophobic fatty acid tails and a hydrophilic phosphate head (Figure 1.1, left). This amphiphilic nature causes phospholipids to spontaneously self-assemble into structures when hydrated to limit the contact between the hydrophobic tails and water. These structures are generally closed and spherical to minimize surface tension. The type of lipid assembly formed widely depends on the geometry of the phospholipid. Amphiphilic molecules with bulky heads

as compared to the tail will tend to assemble into micelles while more cylindrical lipids form a bilayer structure with the hydrophobic heads on both sides of the structure are in contact with water and shield the hydrophobic tails (Figure 1.1, right). Spherical bilayer structures consisting of an aqueous core delimited by the lipid membrane are typically referred to as vesicles, or liposomes when produced artificially (Figure 1.1, right). Liposomes have been widely used in life sciences and biomedical applications as potential drug carriers[2,3], because their size and composition can easily be tuned but also because they have been shown to stabilize drug compounds[7], improve drug dispersion[7], and improve drug uptake[3,7]. They also allow for targeted drug delivery if functionalized accordingly[3,7].

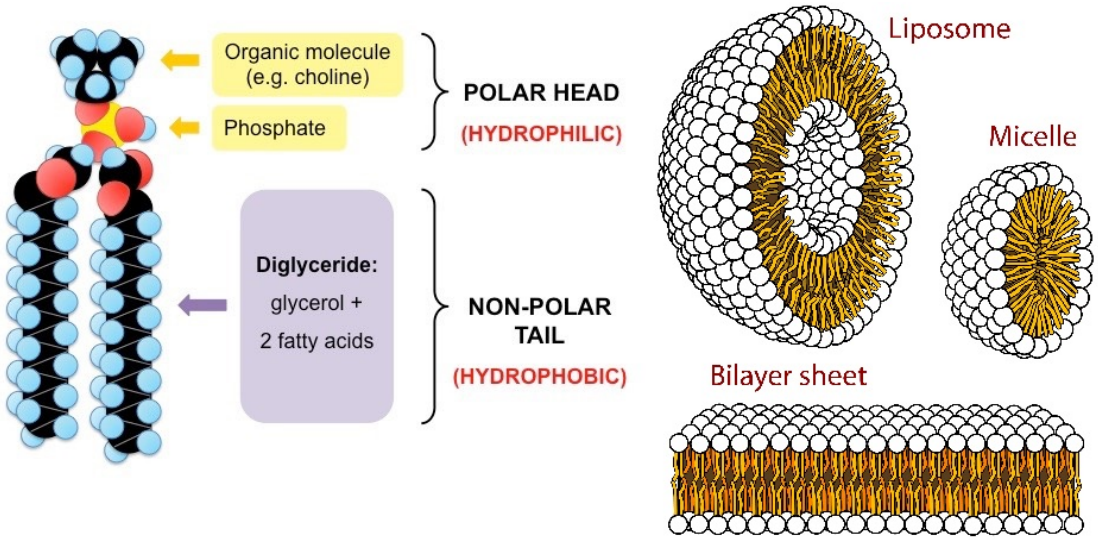

Figure 1.1: *Left: Schematic image of a phospholipid molecule. Cornell, B. (2016) Retrieved from* `http://ib.bioninja.com.au/standard-level/topic-1-cell-biology/13-membrane-structure/phospholipids.html`
Right: Common phospholipid structures. Villareal, M.R. (2007) Retrieved from `https://commons.wikimedia.org/wiki/File:Phospholipids_aqueous_solution_structures.svg`. *Public domain.*

The most noticeable occurrence of phospholipids in nature is in the form of biological membranes, highly complex structures consisting of a phospholipid bilayer embedded with various types of protein and further carrying carbohydrates which serve a variety of functions. Biological membranes separates the cell's interior from the extracellular space and compartmentalizes its interior in various cellular organelles (such as the mitochondria, the endoplasmic reticulum, and the Golgi apparatus). One of the cell membrane's primary function is the trafficking of material in and out of the cell. When taking in material, the cellular membrane will 'bud', bending inwards until finally sealing off (with the aid of membrane proteins), forming a vesicle around the material. On the opposite site, vesicles carrying waste will fuse with the cell membrane, releasing their content to the extracellular space (Figure 1.2, left).

Besides being involved in intracellular trafficking, cells will also secrete vesicles to the extracellular space (Figure 1.2, right). These EVs have attracted significant scientific interest in the recent years[2,3]. They are involved in cell signaling[2,3,8,9], genetic and protein material transfer[2,3,8,9], inflammation response[2,3,8] and tissue regeneration[2]. EV's have

also attracted interest as potential biomarkers for diseases [3,9]. Similarly, many species of bacteria secrete vesicles into the extracellular space. These are known as **o**uter **m**embrane **v**esicles (**OMV**'s), and serve a variety of functions, such as waste disposal, nutritional acquisition, nutritional sharing in bacterial colonies and bacteria-host interaction [10].

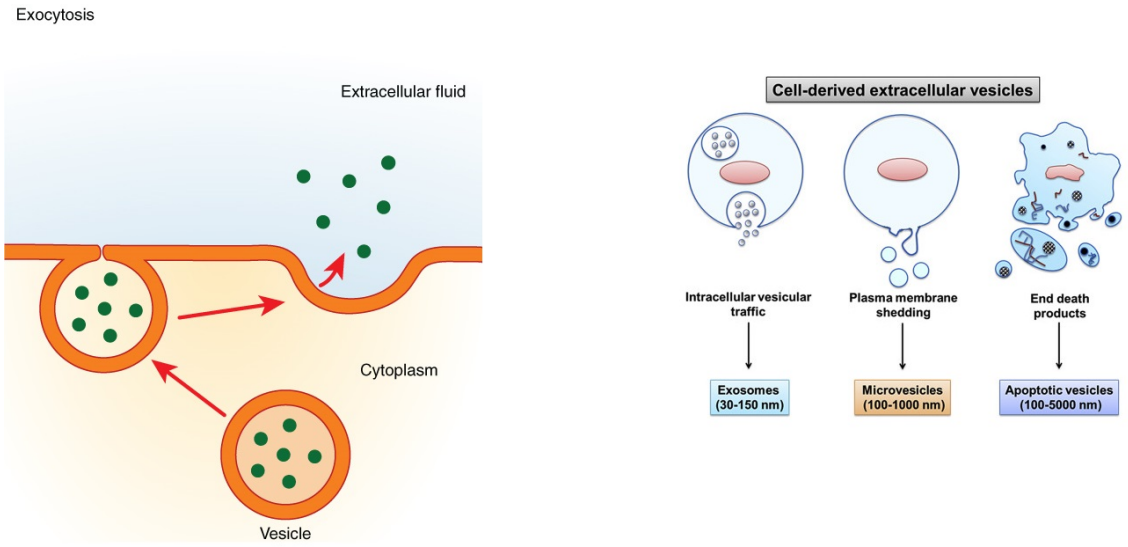

Figure 1.2: *Left: Schematic image of exocytosis. Elias, J. (2018) Grade 11 Biology: Anatomy and Physiology. Retrieved from* `https://cnx.org/contents/AQNhNZty@1.64:q2X995E3@12/The-Cell-Membrane`*. CC BY 4.0*
Right: Three different types of extracellular vesicles. From Devhare, P. B. and Ray, R. B. (2018) Extracellular vesicles: Novel mediator for cell to cell communications in liver pathogenesis. Molecular Aspects of Medicine ***60****, 115-122*

Many species of viruses also possess a phospholipid membrane, a so-called viral envelope surrounding the capsid shell and genetic material [11,12]. These viruses acquire their membrane either from the host's plasma cell membrane or from the membrane of one of its organelles [11]. The viral envelope facilitates entry into the next host cell by promoting attachment to the plasma membrane via biomolecular interactions between biomolecules in the viral envelope and on the cell surface. It also allows for delivery of the viral pay load by fusion with the host cell's membrane prior or after endocytosis [11].

Taken together, lipids and lipid nanoparticle play a key role in a variety of biological processes but also for biomedical applications. In order to study the role and mode of action of vesicles of viruses or to take full advantage of the potential of lipid structures in biomedical applications, new tools to analyze them must be developed and refined.

1.2.2 Particle quantification: nanoparticle tracking analysis

A quantification method for lipid nanoparticles which is currently gaining popularity is NTA. In NTA, a sample is illuminated with a laser beam, and particles in the sample scatter the light, which is then recorded with a camera. By recording the Brownian motion of the particles, the hydrodynamic radius can be determined from the Stokes-Einstein equation, and by analyzing multiple particles a size distribution is obtained. NTA also measures concentrations by simply counting the number of particles in a known volume [5,13,14], allowing NTA to measure both size distribution and concentration concurrently. NTA is

capable of detecting particles down to 10 nm in diameter[14,15], provided that they scatter sufficiently.

NTA has found widespread use in biology, for measuring small particles of biological origin such as various vesicle species[2,5,13,15], viruses[16] and protein aggregates[14]. Compared to alternative methods, the use of NTA to characterize vesicles (and lipid nanoparticles in general) has both advantages and disadvantages. NTA can measure a large quantity of vesicle with relatively little preparation[13], it can measure size and concentration at the same time[5,13–15], it has low detection limit[13], and it can measure polydisperse samples to a reasonable degree[2,14]. A major drawback is however that vesicles have a refractive index close to the one of water, meaning that they will scatter weakly, leading to a practical detection limit around 50-70 nm[2] and a bias towards larger particles in size measurements[14]. This is particularly problematic as both native vesicles and artificial liposomes often have diameters down to 30 nm[3,13,15]. A general problem affecting the field is also the lack of standardized measurement settings[5,15], leading to different devices obtaining different values for same samples and making the comparison of data obtained in different studies difficult.

1.2.3 Phosphorus quantification

One method to be used to quantify nanoparticles made of phospholipids is to quantify the total phosphorus content. Phospholipid molecules contain a single phosphate group in their head-section (Figure 1.1, Section 1.2.1), the phosphorus content can therefore be used to accurately quantify the total phospholipid content.

One chemical approach to quantify the total phosphorus content is the Molybdenum blue method[17,18]. Molybdenum blue is a colorimetric measurement method, in which molybdenum reagent, reductant and strong acid are added to a phosphorus-containing sample, forming polyoxometalate complexes with phosphorus which have a deeply blue color. The intensity of the color is proportional to the total number of complexes, so the total ion content can be measured using absorbance measurements and the Beer's law. The original method described by Murphy and Riley (1958 and 1962) has been refined over the years; we used a method developed by Paraskova *et al.* (2013) in this project.

1.2.4 Colorimetric quantification of protein content

Cell-secreted vesicles are generated from cellular membranes and therefore generally contain proteins embedded in the lipid membrane. Protein quantification therefore represents an alternative method to quantify vesicles of biological origin, and in fact, the total protein content is probably the most commonly used method to provide a quantitative estimate of the vesicle content in exosome-containing samples[2].

To quantify the protein content of a biological sample, a variety of colorimetric assays based on the formation of a colored complex between protein and a reagent have been proposed. The CBQCA protein assay kit used in this work, for example, is a commercially available colorimetric measurements technique to quantify the total protein content of samples. In this case, a 3-(4-**c**arboxy**b**enzoyl)**q**uinoline-2-**c**arbox**a**ldehyde (**CBQCA**) reagent in presence of cyanide will react with amines from proteins to form fluorescent derivates, which can then be measured by fluorometry and related to protein content via a calibration curve. The assay is extremely sensitive, capable of detecting down to 10 ng of proteins in a 200 µL volume[20] and is relatively unaffected by the presence of byproducts, such as lipids[20], making it a particularly good choice for the characterization of lipid vesicles.

1.2.5 Förster Resonance Energy transfer

Förster **R**esonance **E**nergy **T**ransfer, or **FRET** is one of the many fluorescence principles that has found a variety application in methods for biological sciences. FRET occurs if two fluorophores with overlapping spectral properties are found close to each other. Indeed, if an excited fluorophore (usually designated as the **donor**) is in close proximity to an **acceptor** fluorophore whose excitation spectrum overlaps with the emission spectrum of the donor, there is a chance for the excitation energy to be transferred from donor to acceptor, which then radiates the energy. This energy transfer is non-radiative, but rather the result of a dipole-dipole interaction between the fluorophores.

The efficiency E of FRET is extremely sensitive for the distance r between the donor and the acceptor fluorophores, with the relation given by [21]

$$E = \frac{1}{1 + (\frac{r}{R_0})^6}$$

where R_0 is a constant unique for different donor-acceptors, called the 'Förster distance' and represents the distance at which the efficiency is 50 %.

Due to this extreme distance sensitivity of FRET efficiency, and the length scale of the Förster distance, which is usually in the range of 20-60 Å [21], FRET can be used to measure distances on a molecular level and is sometimes referred to as a 'spectroscopic ruler' [22]. Accordingly, FRET serves as a useful measurement tool in molecular biology, for example in the context of detecting changes in protein conformation [23,24], of measuring protein-protein interactions [23,24] and probing enzyme activity detection [25], with FRET serving both as a qualitative (i.e. confirm binding) and quantitative (i.e. measuring distance) measurement technique. In particular, FRET has also been used in membrane fusion assays, to detect membrane fusion between labeled lipid vesicles and unlabeled lipid vesicles or cellular membranes [26–28]. This will be covered in more detail in Chapter 2.

2

Aim of the thesis: To develop FRET based assay for surface area quantifications

In view of the wide range of biological functions ascribed to lipid vesicles and of the broad interest of in biomedical applications, methods to characterize accurately vesicle-containing samples are urgently needed.

The aim of this thesis was therefore to develop and validate a new method for the quantification of lipid nanoparticles. The method is based on measuring the total membrane surface area of a sample by fusing vesicles containing a FRET-donor and a FRET acceptor fluorophore with the lipid nanoparticle sample to be characterized.

Approach

The study of membrane fusion with FRET was first demonstrated Vanderwerf & Ullman (1980). The method was further expanded upon by Struck *et al.* (1981). The principle behind the method used by Struck *et al.* is used in this thesis.

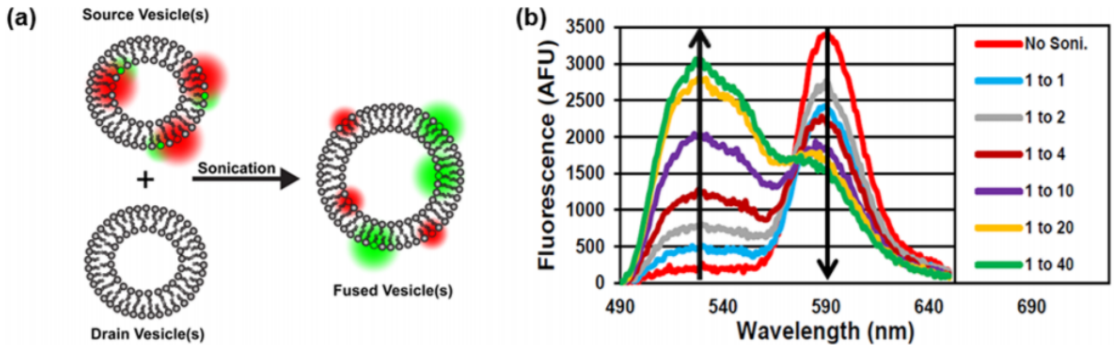

Figure 2.1: *Schematic representation of the FRET assay. (a): Source vesicles labeled with a FRET pair fuse with unlabeled drain vesicles, reducing the surface density of fluorophores. (b): Shift in fluorescence due to the lower fluorophore surface density. Higher ratio of drain vesicles results in larger shifts. From Pace et al. (2015).*

A schematic image of the assay strategy proposed in this thesis can be seen in Figure 2.1. The method uses synthetic vesicles labeled with a fluorophore pair ('source vesicles' in Figure 2.1) subject to FRET. The fluorophore content is high enough that the donors and acceptors are in close proximity to each other and the fluorescent spectra is dominated

by the signal from the acceptor fluorophore. This FRET-vesicle solution is then mixed with an unknown vesicle solution to be quantified ('drain vesicles' in Figure 2.1) and fused together by sonication. After fusion, the surface density of the fluorophore has decreased, increasing the distance between the fluorophore pair, which decreases the FRET-efficiency. This causes a shift in the spectrum of the sample; the signal from the acceptor decreases and the signal from the donor increases, with higher amounts of drain vesicles resulting in a greater shift (see Figure 2.1 on the right). It can therefore be hypothesized that such an approach can be used to provide a quantitative estimate of the total surface area of the drain vesicle sample as originally suggested by Pace *et al.*[28,29]. To take advantage of this idea, our approach is based on first establishing a calibration curve showing the peak ratio as a function of the source vesicle percentage using known concentrations of source and drain vesicles. A vesicle sample with unknown concentration can then be quantified by fusing them with the source vesicles and comparing the peak ratio to the calibration curve.

In this thesis, we investigate and validate this method to determine whether it serves as a viable method to quantify the amount of membrane material in an unknown sample. More specifically, we wish to examine whether we can correlate the change in peak ratio of the fluorophore pair after sonication to the surface area of the unknown sample and whether this can be done on different types of lipid nanoparticles, both of synthetic vesicles containing cholesterol and nanoparticles of biological origin; outer membrane vesicles from *E. coli* bacteria, and membrane enveloped viruses. We further wish to compare the performance of our method to established alternative measurements techniques allowing for the quantification of vesicle samples. For this project we used nanoparticle tracking analysis, phosphorus quantification and protein quantification as comparison methods.

3

Materials & methods

3.1 Materials

Lipids

Lipids used in this project were 1-**p**almitoyl-2-**o**leoyl-SN-glycero-3-**p**hospho**c**holine (**POPC**), 1,2-dioleoyl-sn-glycero-3-**p**hospho**e**thanolamine-N-(lissamine **rhod**amine B sulfonyl) (**Rhod-PE**, Ex/Em: 560/583 nm), 1,2-dioleoyl-sn-glycero-3-**p**hospho**e**thanolamine-N-(7-**n**itro-2-1,3-**b**enzoxa**d**iazol-4-yl) (**NBD-PE**, Ex/Em: 460/535 nm), N-(Lissamine rhodamine B sulfonyl)-1,2-**di**h**h**exadecanoyl-sn-glycero-3-**p**hospho**e**thanolamine, triethylammonium salt (Rhod-**DHPE**, Ex/Em: 560/583 nm) and cholesterol. Chloroform (CHCl3) was used as a solvent for all lipids. All lipids except for cholesterol were obtained from Avanti Polar Lipids Inc. (Alabama, USA). Cholesterol and chloroform were obtained from Sigma-Aldrich (Darmstadt, Germany).

Buffers

Two buffers were used in the project, **H**EPES **b**uffered **s**aline (**HBS**), consisting of 10 mM 4-(2-**h**ydroxy**e**thyl)-1-**p**iperazine**e**thane**s**ulfonic acid (**HEPES**) and 150 mM NaCl, with pH = 7,4, and **p**hosphate **b**uffered **s**aline (**PBS**) obtained from tablets. HEPES was obtained from Merck (New Jersey, USA), PBS tablets were obtained from Medicago AB (Uppsala, Sweden), and NaCl was obtained from VWR Chemicals (Leuven, Belgium).

Phosphorus assay

Potassium antimonyl tartrate trihydrate ($C_8H_4K_2O_{12}Sb_2 \cdot 3H_2O$), ammonium heptamolybdate tetrahydrate ($(NH_4)_6Mo_7O_{24} \cdot 4H_2O$) and a phosphorus standard solution (0,65 M) were obtained from Sigma-Aldrich. Sulfuric acid (H_2SO_4) and ascorbic acid ($C_6H_6O_6$) were obtained from Merck.

CBQCA protein assay kit

CBQCA protein assay kit was obtained from Thermo-Fisher Scientific (Massachusetts, USA).

Outer membrane vesicles

Two types of OMV's from *E. coli* bacteria, one from **w**ild **t**ype (**WT**) and the other from **hldE** mutant with truncated lipopolysaccharide outer membrane, were kindly provided by Madeleine Ramstedt (Department of Chemistry, Umeå University).

Virus

Herpes **s**implex **v**irus type **2** (**HSV-2**) samples were kindly provided by Tomas Bergström (Department of Infectious Diseases, University of Gothenburg).

3.2 Vesicle preparation

All vesicles were prepared using the lipid hydration and extrusion method. Appropriate amounts of lipids dissolved in chloroform were added to a round-bottom flask. The chloroform is first evaporated under a constant airflow while rotating the flask at an angle to form a homogeneous lipid film on the bottom of the flask. The flask was then left under airflow for 1 hour to ensure that all the chloroform evaporates. After drying, the lipid film was hydrated with an aqueous buffer and extruded through a polycarbonate membrane with 100 nm pores eleven times using a miniextruder (Avanti Polar Lipids Inc.). All vesicles were made in HBS unless otherwise specified.

We prepared a 1 mg/mL FRET vesicle solution, consisting of 99 mol% POPC, 0,5 mol% Rhod-PE and 0,5 mol% NBD-PE, to use as source vesicles in the FRET assay. For calibrating the assay and testing sonication parameters, we prepared a 2 mg/mL POPC vesicle solution. We also prepared a solution of cholesterol-containing POPC vesicles (molar ratio 1:1) at 1 mg POPC/mL to test in the FRET assay.

To test the influence of sonication procedure on fluorescence we prepared a 1 mg/mL vesicle solution consisting of 99,8 mol% POPC, 0,1 mol% Rhod-DHPE (lab was out of Rhod-PE when these vesicles were made) and 0,1 mol% NBD-PE. This was the only vesicle species produced in PBS as a buffer (instead of HBS).

3.3 Phosphorus assay

To quantify the phospholipid content of our vesicle stocks, a phosphorus assay was used. The assay was based on a method from Paraskova *et al.* (2013), which is based on the molybdenum blue method[17,18]. The method involves mixing two reagents with a phosphorus containing sample. Reagent 1 consists of

- 1 part potassium antimonyl tartrate trihydrate ($C_8H_4K_2O_{12}Sb_2 \cdot 3H_2O$) at 1 mg Sb/mL
- 3 parts ammonium heptamolybdate tetrahydrate ($(NH_4)_6Mo_7O_{24} \cdot 4H_2O$) at 4 %
- 10 parts hydrosulfuric acid (H_2SO_4) at 2,5 M.

Reagent 2 is 0,1 M ascorbic acid ($C_6H_6O_6$). 98 % pure hydrosulfuric acid was diluted to 2,5 M; all other chemicals were obtained in powder form and dissolved in appropriate amounts in MQ water. To perform the assay, a sample containing between 0-100 nmol of phosphorus was calcinated at 550°C for at least 4 hours in a Carbolite CWF 1200 furnace (Carbolite Gero Limited, Hope Valley, UK). After calcification, the resulting ashes were dissolved in 4 mL MQ water. Then 1 mL mixture, consisting of seven parts reagent 1 and three parts reagent 2, was added to each sample. After adding the mixture, the sample was incubated for at least 15 minutes. After incubating, 150 µL of each sample was added to a well of a clear U-bottomed polystyrene NUNC plate (Cat. no. 650 101, Greiner Bio One International GmbH, Kremsmünster, Austria) and absorbance at 882 nm was measured in a spectrofluorometer (Varioskan Flash, Thermo Fisher Scientific). We

measured absorbance three times to obtain an average. The bandwidth of measurement was 5 nm and measurement time was 100 ms. The absorbance was then compared to a calibration curve to assess the phosphorus content. We established calibration curves for the assay using a 0,65 mM phosphorus standard solution. The calibration curve was established without calcinating the standard solution, as a preliminary test showed no difference in the absorbance between calcinated and uncalcinated standard solution.

3.4 Nanoparticle tracking analysis

All vesicle species were analyzed with NTA. Measurements were performed with ZetaView PMX 110 NTA device from Particle Metrix GmbH (Inning am Ammersee, Germany). The device is calibrated with 102 nm standard beads from the manufacturer before measurements. 'Sensitivity' and 'Shutter' parameters were determined to have optimal values 'Sensitivity' = 75 and 'Shutter' = 35, based on manufacturer's guidelines and after testing different parameters on our POPC vesicle sample. Samples were diluted to an optimal concentration for analysis (between 100-200 visible particles) and ~800 µL of the sample were injected into the measurement chamber and measured. The device performs measurements at 11 different positions in the measurement chamber and gives an average as a result. Each vesicle species was measured in triplicate to obtain an average.

3.5 CBQCA protein assay kit

The protein content of the OMV's and viral samples was measured with a CBQCA protein assay kit. All components except MQ water and sodium borate buffer were included in the kit. A standard curve was made using bovine serum albumin (10 µg/mL) standard included in the kit. 100 mM sodium borate buffer (pH = 9,3) was used as buffer for samples.

500 µL of 5 mM CBQCA stock in sodium borate were prepared. The content of a standardized vial of CBQCA was dissolved in 410 µL DMSO solvent. 62,5 µL of this solution were then diluted in 437,5 µL sodium borate buffer.

20 mM KCN solution was made by dissolving 20 mg KCN powder in 17 µL MQ water.

Samples to be measured are made by mixing 10 µL CBQCA, 5 µL KCN, and appropriate amount of sample and sodium borate buffer for a final volume of 150 µL in Eppendorf tubes. OMV's were measured at two volumes, 5,7 µL and 57 µL for hldE, and 18,5 µL and 185 µL for WT. Viral samples were measured at two volumes, 13 µL and 26 µL. After mixing, the samples are incubated on a platform shaker for one hour. After incubation, 100 µL of sample are added to the well of a black-bottomed NUNC plate (634-0006, Thermo Scientific) and measured with the spectrofluorometer. We excite the samples with 465 nm light and measure the response at 550 nm. The excitation bandwidth was 12 nm, dynamic range was set to 'Medium Low' and measurement time was 100 ms. For all measurements (including calibration) we subtract the signal of a blank sample to correct for background. Calibration curve for the assay can be seen in Supplement B.

3.6 Sonication procedure

Unless stated otherwise, the FRET assay was performed as follows: source (FRET) vesicles, drain vesicles and HBS are mixed in Eppendorf tubes. The concentration of FRET

vesicles was kept constant at 0,033 mg/mL while the concentration of drain vesicles was varied according to needs. To do so, 2 µL of FRET vesicles (1 mg/mL) were mixed with appropriate volume of drain vesicles and buffer to reach a total volume of 60 µL. The volume was kept constant for all measurements to ensure reproducibility of the sonication procedure. The Eppendorf tubes were sealed with parafilm to avoid opening during sonication.

Before sonicating samples, the sonicator must be warmed up to the operational temperature. The water in the sonicator must also be degassed by letting the sonicator run for at least 20 minutes before sonicating samples (otherwise vibrations are too weak to obtain sufficient fusion). The water level in the sonicator was kept slightly above half-full when operating (similar to the level seen in Figure 3.1 A). When sonicating, the samples were placed at vibrational 'hotspots', where the vibrations are strongest, generally around the middle of the sonicator (varies between sonications, see Figure 3.1 B). When running, the water temperature tends to increase due to the vibrations; ice was therefore added regularly to maintain operation temperature. Every quarter of sonication time, the sample holder was rotated 90 degrees to ensure that all samples were evenly sonicated (up to 3 Eppendorfs were sonicated at the same time). After sonication the samples were quickly centrifuged to condense the liquid in the tubes. Between sonications and spectrofluorometric measurements, the samples were stored at 5°C.

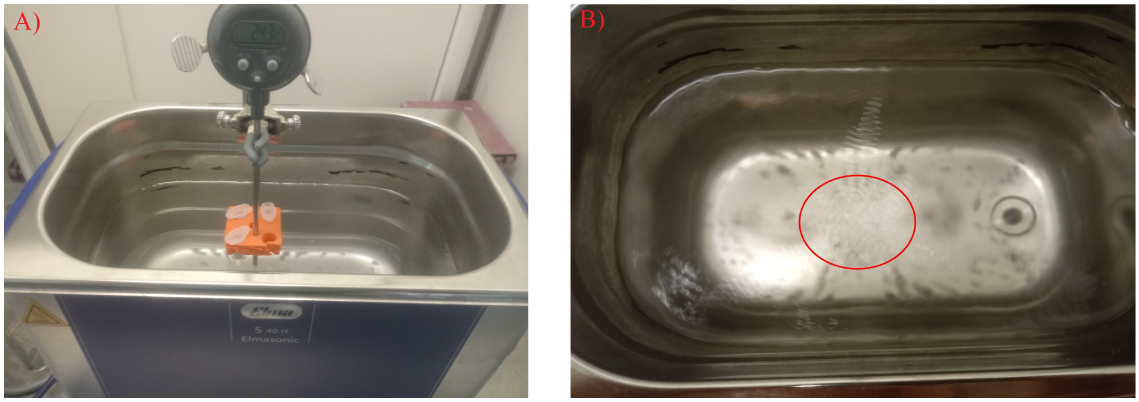

Figure 3.1: *A) Sonicator setup. Samples are placed in sample holder (orange) which is mounted on the thermometer. B) A vibrational hotspot seen in the sonicator during sonication.*

For fluorescence measurements, 50 µL of the sonicated samples were mixed with 50 µL buffer in the well of a black-bottomed NUNC plate (634-0006, Thermo Scientific) and scanned with the spectrofluorometer. To acquire an emission spectrum, the samples were excited at 460 nm and the fluorescent intensity response measured in the range 490-650 nm. Excitation bandwidth was 12 nm and dynamic range set to 'Medium Low'. Measurement time was 100 ms. In all measurements, the background signal of pure buffer was subtracted from the FRET signal. Rhodamine and NBD have listed spectral intensity peaks at 583 and 535 nm respectively. Based on our data, the intensity peaks are located at 588 nm for Rhodamine and 535 nm for NBD. These wavelengths were therefore used to estimate the respective peak intensity values.

3.6.1 Sonication parameter analysis

Effects of sonication parameters on FRET fluorescence

To test the effects of sonication time and temperature on FRET fluorescence, we prepared a 1 mg/mL vesicle solution in PBS consisting of 99,8 mol% POPC, 0,1 mol% NBD-PE and 0,1 mol% Rhod-DHPE. Measurements were performed using 10 µL of these vesicles in 50 µL of buffer. Temperature measurements were performed at 20, 40, 60 and 80°C with sonication time fixed at 10 minutes. Time measurements were 5, 10, 20 and 30 minutes with temperature fixed at 20°C. For each datapoint, three samples were sonicated to obtain an average, with the standard deviation as error. After sonications the fluorescence intensity was measured.

Effects of sonication parameters on vesicle fusion

To assess the effects of sonication time and temperature on vesicle fusion, we ran the assay at a constant vesicle concentration, using 10 µL of POPC vesicles in HBS (2 mg/mL) as described in the beginning of Section 3.6. We varied sonication times (with temperature fixed) and varied temperatures (with sonication time fixed). Vesicle fusion efficiency was evaluated based on the intensity peak ratio shift (Rhod/NBD). For each datapoint, three samples were sonicated to obtain an average, with the standard deviation as error. After sonications the fluorescence intensity was measured.

3.6.2 Calibration curves

We created a calibration curve for the FRET assay for use in surface area quantifications. The curve was made by sonicating varying FRET/POPC vesicle ratios and measuring the peak ratio between the rhodamine and the NBD. POPC vesicles used for measurements were 2 mg/mL (as determined by the phosphorus assay) in HBS, and samples contained between 0,5 µL and 8 µL. Based on the results of sonication parameter analysis (see Sections 4.1.2 - 4.1.3), sonication time was 20 minutes and sonication temperature was 40°C for all sonications. For each datapoint, three samples were sonicated to obtain an average. After sonications the fluorescence intensity was measured.

3.6.3 Quantification of vesicle species

Cholesterol-containing POPC vesicles

We performed a volume gradient by sonicating different volumes (2-16 µL) of cholesterol-containing vesicles at 40°C to confirm fusion with FRET vesicles and to find optimal volume for quantification. Temperature analysis was performed by sonicating 8 µL of cholesterol-containing vesicles at 20, 40, 60 and 80°C. For each datapoint, three samples were sonicated to obtain an average, with the standard deviation as error. All sonications were 20 minutes. Quantifications were made using the 2 µL volume measurements.

OMV's

We performed a volume gradient for both OMV species by sonicating different volumes (15-45 µL) of OMV's at 40°C to confirm fusion with FRET vesicles and to find optimal volume for quantification. In this case, a single measurement was performed for each

dilution. Temperature analysis was performed by sonicating fixed volume of OMV'S (20 µL for hldE, 30 µL for WT) at 20, 40, 60 and 80°C. For each temperature, three samples were sonicated to obtain an average, with the standard deviation as error. All sonications were 20 minutes. Quantifications were made with the results from temperature measurements at 40°C.

HSV-2 viral samples

Viral samples were stored at -80°C, so before measurements samples were thawed at room temperature for 30 minutes. We performed a volume gradient by sonicating different volumes (10-30 µL) of viral solution to confirm fusion with FRET vesicles and to find optimal volume for quantification. Temperature analysis data was obtained from previously performed measurements Chalmers (see section 4.1.3) and optimal sonication temperature was found to be 80°C. All sonications were therefore 20 minutes at 80°C. Quantifications were made by sonicating 30 µL in triplicate to obtain an average, with the standard deviation as error.

4

Results

4.1 Establishing calibration curves

As detailed in Chapter 2, the principle of the proposed FRET assay is to accurately quantify membrane surface area of lipid membrane samples by inducing fusion, via sonication, between source vesicles containing a FRET fluorophore pair and drain vesicles, whose concentration is to be determined. The **s**urface **a**rea **c**oncentration (**SAC**, nm^2/mL) is then determined using a calibration curve obtained from a standard sample with known SAC. The first step in establishing the method was therefore to test the assay on drain vesicles with known SAC's, establishing a calibration curve to be used as a reference for measurements of unknown samples.

4.1.1 Preparation and characterization of FRET and POPC vesicles

Our lipid of choice to establish the calibration curve for the FRET assay (for both source and drain vesicles) was POPC. This choice is motivated by the fact that phosphocholine lipids are commonly found in cell membranes and often used in the context of artificial model membranes. For the FRET source vesicles, the fluorophore pair used was rhodamine and NBD. We prepared FRET vesicles consisting of 99 mol% POPC, 0,5 mol% Rhod-PE and 0,5 mol% NBD-PE.

Both the FRET source vesicles and the POPC drain vesicles were prepared by extrusion. We prepared a 1 mg/mL FRET vesicle solution to use as source vesicles and 2 mg/mL POPC vesicle solution to use as drain vesicles for calibration.

Verification of lipid concentrations

In order to trust the assay, we must be certain of the lipid material concentrations of the calibration vesicles. The largest concern regarding accuracy of concentrations is the potential loss of material in the polycarbonate membranes during extrusion. Specifically, to ensure that our FRET assay is accurate, we need to know the lipid concentration of the FRET and POPC vesicle suspensions. We therefore did independent quantifications on both species using phosphorus quantification and nanoparticle tracking analysis.

Phosphorus quantification

One method to quantify the lipid content of a vesicle suspension is to quantify the total phosphorus content. Indeed, phospholipids contain a hydrophilic phosphate head, and therefore a single phosphorus atom so that the phospholipid content can be directly determined by measuring the phosphorus content. In this project, we used a method based on the molybdenum blue method [19] to measure the phosphorus content of our samples. We

created a calibration curve using a phosphorus standard solution, which was then used as a reference to quantify the phosphorus content of our vesicle samples. In Figure 4.1 we see the calibration curve for the phosphorus assay, obtained from three independent measurements. The graph shows good linearity between absorbance and phosphorus content for the tested range. The intercept of the y-axis deviates slightly from zero; this is most likely due to trace quantity of phosphorus in the MQ-water used in the assay. Since our vesicle solutions use the same water, this error is systematic and shouldn't affect quantifications.

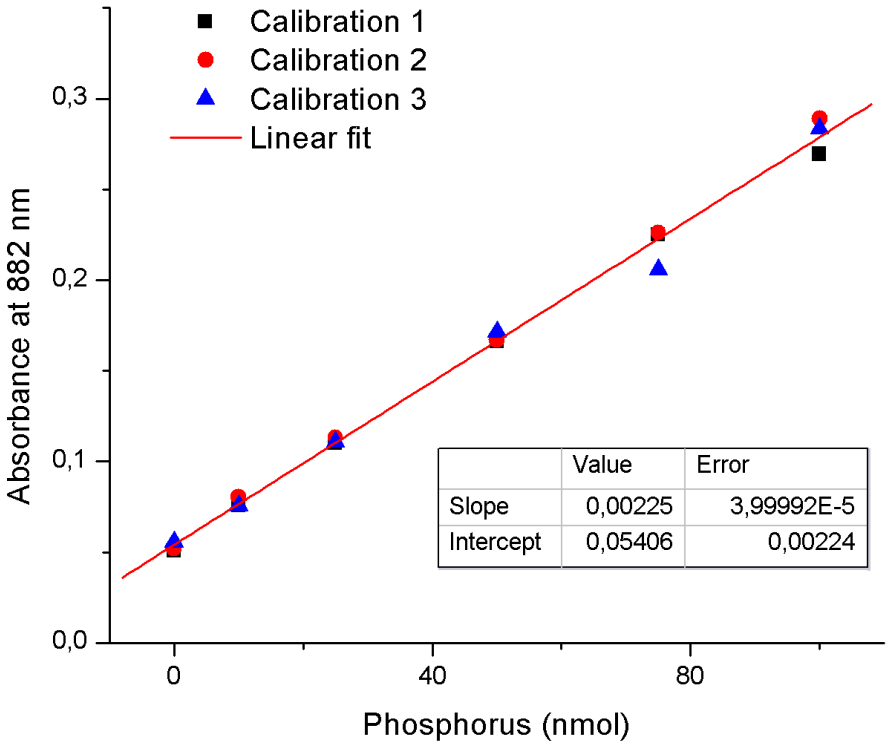

Figure 4.1: *Calibration curve for the phosphorus assay. Data obtained from three separate measurements.*

Table 4.1: *Lipid concentrations from the phosphorus assay compared to theoretical values. All phosphorus assays were performed in triplicates, errors are the standard deviations.*

	Theoretical lipid conc. (mg/mL)	Phosphorus assay conc. (mg/mL)
FRET vesicles	1	$0,86 \pm 0,17$
POPC vesicles	2	$1,81 \pm 0,14$

We quantified the phosphorus content of our FRET and POPC vesicles, and from that derived the total lipid content; results can be seen in Table 4.1. The results indicate that

some amount of material is lost, as compared to the expected lipid content of the vesicles based on the amount of lipid material added to the preparation (theoretical value). This is attributed to material loss in the polycarbonate membranes used during extrusion. The material lost is 9,5 % for the FRET vesicles and 14 % for the POPC vesicles.

Nanoparticle tracking analysis

Another method for quantifying particle suspensions is NTA. By directly counting the number of particles in a known volume of sample and measuring their diameter, we can, using this method, calculate the total SAC. Using the area-per-lipid of POPC molecules (0,63 nm^2 [30]) we can then estimate the total lipid content of the sample (by reversing the calculations seen in Supplement A.1). In Figure 4.2, we see the size distributions for the FRET and POPC vesicles obtained by NTA. Based on the size distribution, we evaluated the mean diameter of the vesicles and the total SAC. Results of this analysis can be seen in Table 4.2.

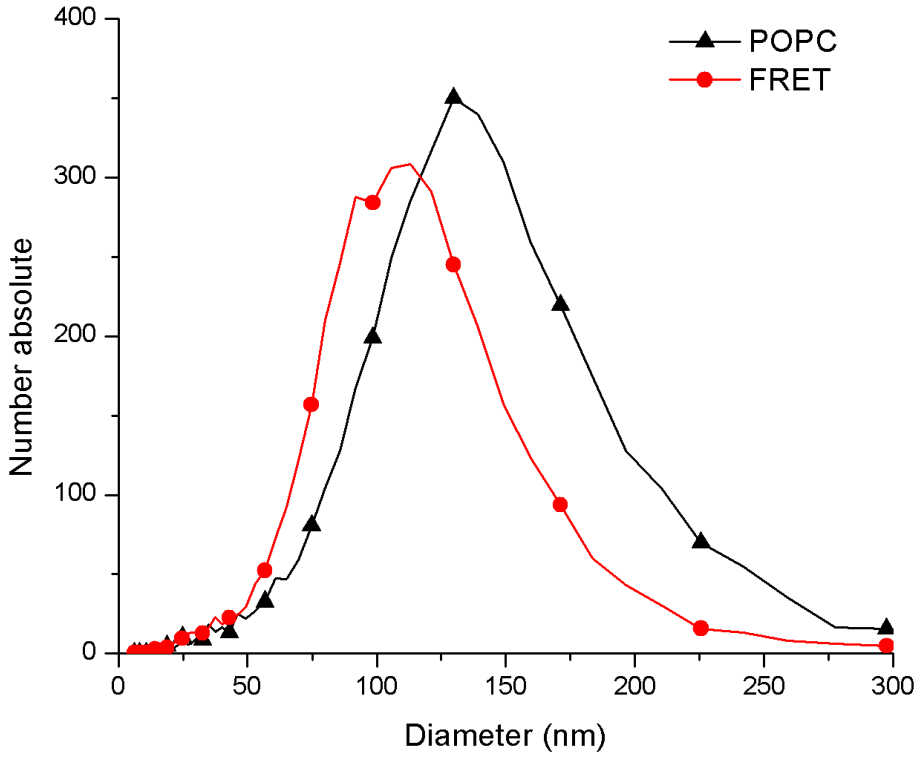

Figure 4.2: *NTA size distribution for the FRET and POPC vesicles. The mean diameter and particle concentration are measured by the device and used to determine the SAC (note that the mean diameter is different from the peak diameter, visible on the graphs).*

Table 4.2: *Numerical data from the NTA. Mean diameter and particle concentration are measured directly by the NTA device, which can then be used to calculate the SAC and lipid concentrations.*

	Mean diameter (nm)	Particles/mL ($\times 10^{12}$)	SAC (nm^2/mL $\times 10^{17}$)	Lipid conc. (mg/mL)
FRET vesicles	131 ± 3	$0,913 \pm 0,074$	$0,655 \pm 0,042$	$0,262 \pm 0,017$
POPC vesicles	124 ± 1	$1,986 \pm 0,012$	$1,265 \pm 0,062$	$0,507 \pm 0,025$

As often reported in literature [31], the mean diameter of our vesicles is considerably higher than the pore size of the polycarbonate membranes used for extrusion. This is not unusual; lipid nanoparticles are not rigid but can deform to fit through tight openings. The concentrations on the other hand are significantly lower than expected, almost quarter the expected value, indicating that most likely the NTA device is not sensitive enough to detect the smallest vesicles in the sample, as reported by others [2,4,5]. An analysis was made on the POPC vesicles with two other NTA devices, with each device giving different results for the lipid concentrations (see Supplement C), further suggesting that sensitivity issues may be affecting the measurement. On the other hand, it is important to stress that the relative values are reasonable, with POPC vesicles having twice the concentration of FRET vesicles, as expected.

4.1.2 The effects of sonication parameters on FRET fluorescence

A practical aspect to be considered when establishing our quantification method, is whether the fluorophores themselves are affected by the sonication process. In particular, we must determine whether the peak ratio between the rhodamine peak and the NBD peak is affected by the sonication procedure. If so, this will have to be accounted for when comparing different sonication conditions and when establishing calibration curves. If the results vary considerably, the assay may need to be calibrated for multiple experimental procedures.

For these measurements, we sonicated fluorescent vesicles only (no drain vesicles) and used a FRET vesicle suspension with a 10-times lower fluorophore concentration than normally used in the assay, i.e. with reduced energy transfer between the fluorophores. Specifically, at this concentration, the rhodamine and NBD peaks have similar fluorescence intensity, allowing us to better detect peak ratio shifts. We sonicated our FRET-vesicles at different temperatures with sonication time fixed at 10 minutes, and different sonication times with temperature fixed at 40°C. We then evaluated the peak ratio of the rhodamine peak and the NBD peak and plotted as a function of the respective parameter. Results can be seen in Figure 4.3.

Our results indicate that sonication time has no discernible effect on fluorescence intensity, and accordingly the peak ratio stays constant. On the other hand, sonication temperature significantly affects the emitted fluorescence intensity; it drops as the temperature rises to 40°C, then rises. Nevertheless, the peak ratio remains relatively stable for all temperatures except 80°C, where it is slightly higher, although not enough to affect quantification measurements to any serious degree.

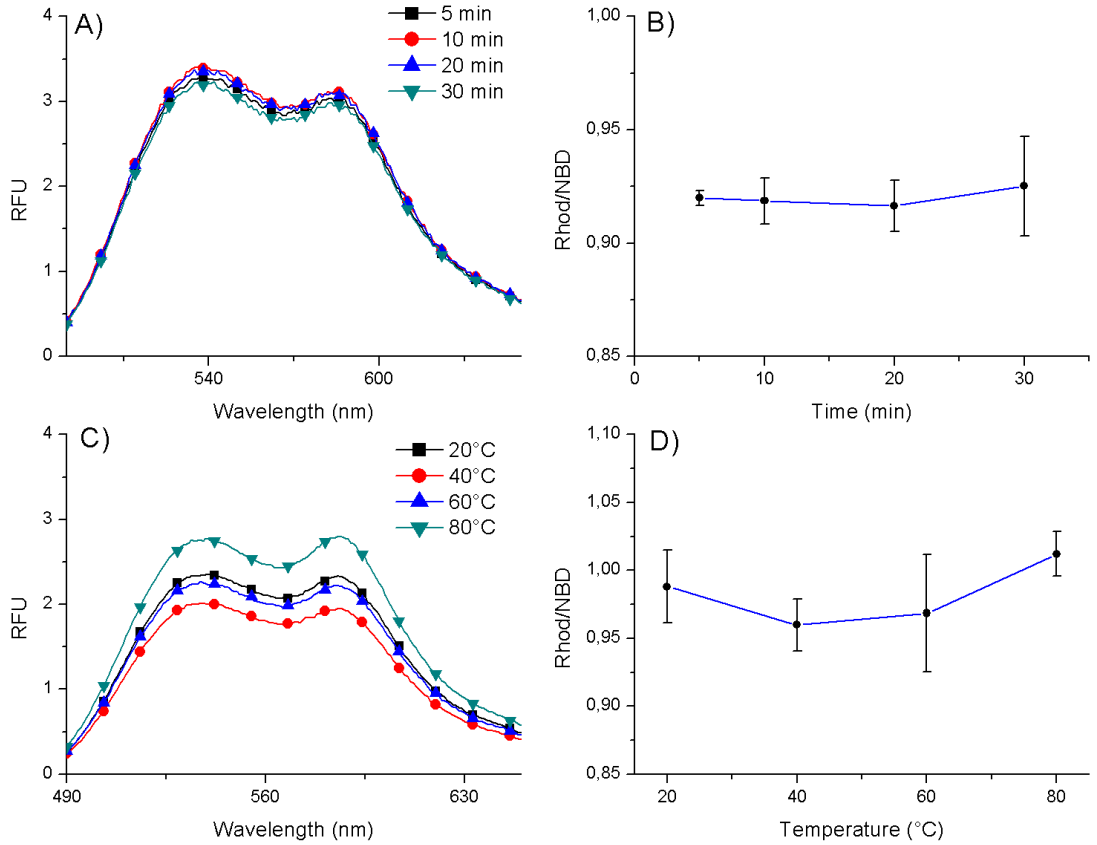

Figure 4.3: *A) Fluorescence emission spectra for different sonication times, with temperature fixed at 40°C. B) Peak ratio as a function of sonication time. C) Spectra for different sonication temperatures, with sonication time fixed at 20 minutes. D) Peak ratio as a function of sonication temperature. All spectra are the average of three samples. Peak ratios are the average of the three spectra, with standard deviation as the error.*

4.1.3 Effects of sonication parameters on vesicle fusion

The proposed assay strategy relies on the assumption that complete mixing between drain and source vesicles is achieved. To accurately quantify vesicles, we must therefore also assess if and how sonication procedure parameters affect the efficiency of vesicle fusion and choose a combination of sonication time and temperature which ensures maximal fusion. To determine the minimal conditions to obtain maximal mixing, we performed the assay using a fixed FRET/POPC vesicle ratio and sonicated at different temperatures and sonication times (keeping the other parameter fixed) to assess the fusion efficiency. The results can be seen in Figure 4.4.

Results indicate that for the POPC vesicles, temperature has minimal to no effect on vesicle fusion efficiency. This means the assay can be calibrated at a single temperature and be valid for quantifications performed at any temperatures. On the other hand, fusion efficiency increased with sonication time, reaching a maximum at t> ∼15 min. Based on these results, in order to obtain optimal vesicle fusion, sonications need to be performed for at least 20 minutes. Having determined that the peak ratio is independent of the sonication parameters and that maximal mixing was obtained for sonication times

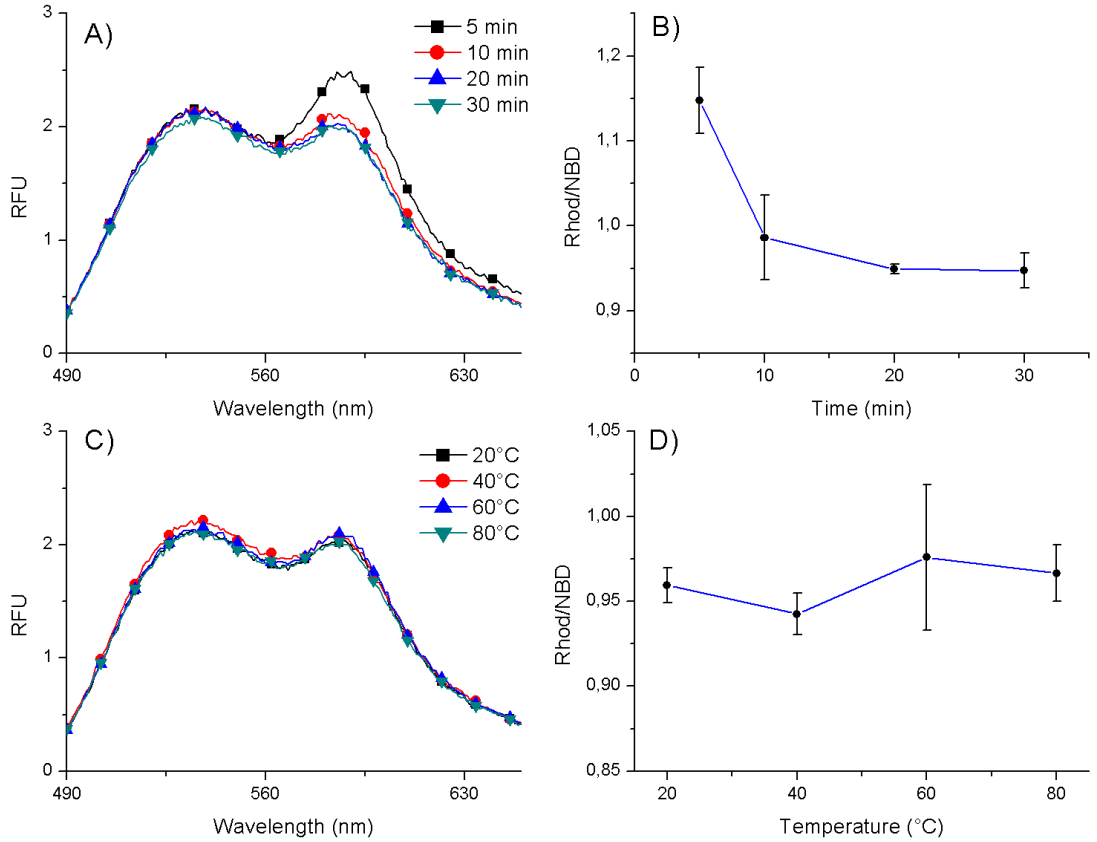

Figure 4.4: *A) Fluorescence emission spectra for different sonication times, with temperature fixed at 40°C. B) Peak ratio as a function of sonication time. C) Fluorescence emission spectra for different sonication temperatures, with sonication time fixed at 20 minutes. D) Peak ratio as a function of sonication temperature. All spectra are the average of three samples. Peak ratios are the average of the three spectra, with standard deviation as the error.*

$\leq$ 20 min, we therefore settled on 20 minutes for sonication time and 40°C for sonication temperature to obtain all calibration curves used in this project.

4.1.4 Calibration curves for the FRET assay

Having determined which sonication parameters are optimal for membrane fusion, we calibrated the FRET-assay. To do so, we sonicated varying ratios of FRET/POPC vesicles where the FRET vesicle content was kept constant. We then determined the peak ratio between the spectral peaks of rhodamine and NBD. The peak ratio was then plotted as a function of the surface area fraction of the FRET vesicles (designated '**FRET-fraction**' on the graphs) given by

$$\text{FRET} - \text{fraction} = \frac{A_{FRET}}{A_{FRET} + A_{drain}}$$

where A_{FRET} is the total surface area of the FRET vesicles and A_{drain} is the total surface area of the drain vesicles in the sample. The SAC of a reference sample made of well-characterized lipids can be determined from the mass concentration (mg/mL) by using literature value for the area-per-lipid of the relevant phospholipid (in our case POPC) as further detailed in Supplement A.2. However, when using POPC vesicles for calibration, since the FRET vesicles are also made of POPC, and since we can assume that the fluorophores have minimal effects on surface area, this can be simplified to the mass fraction of FRET vesicles:

$$\text{FRET} - \text{fraction} = \frac{m_{FRET}}{m_{FRET} + m_{POPC}}$$

where m_{FRET} and m_{POPC} are the masses of the FRET and POPC vesicles in the sample respectively. We started by performing the FRET assay for FRET-fractions between 0 and 1 to determine the linear region of the assay and to examine the endpoint behavior. In Figure 4.5 we see that the curve can be approximated by a linear fit at FRET-fractions ranging from 0,2 to 0,8. The linear region corresponds to intensity peak ratios between 1 – 3,5. At FRET-ratios > 0,8 (corresponding to low POPC content), the data bends upwards away from the linear region. Based on this information, we create a calibration curve for use in quantifications focusing on the linear region (Figure 4.6).

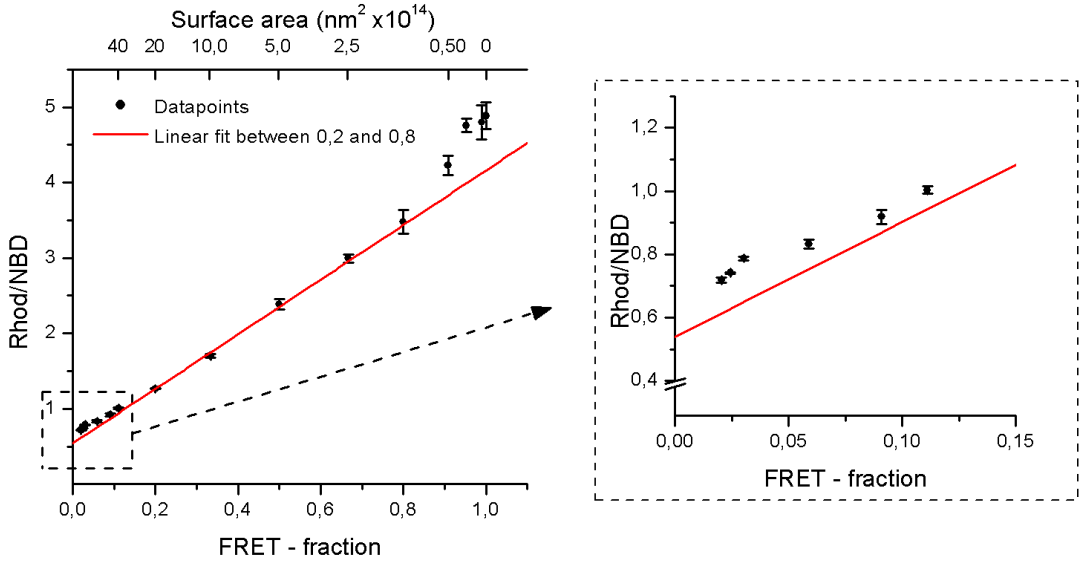

Figure 4.5: *FRET assay between 0 and 1, along with a zoomed in view of the region between FRET-fractions 0 to 0,15. Drain vesicle surface area can be seen on the top axis. Linear fit is made of datapoints in the FRET-fraction interval 0,2 to 0,8. All datapoints are the averages of three independent measurements of the vesicle reference sample, with standard deviations as errors.*

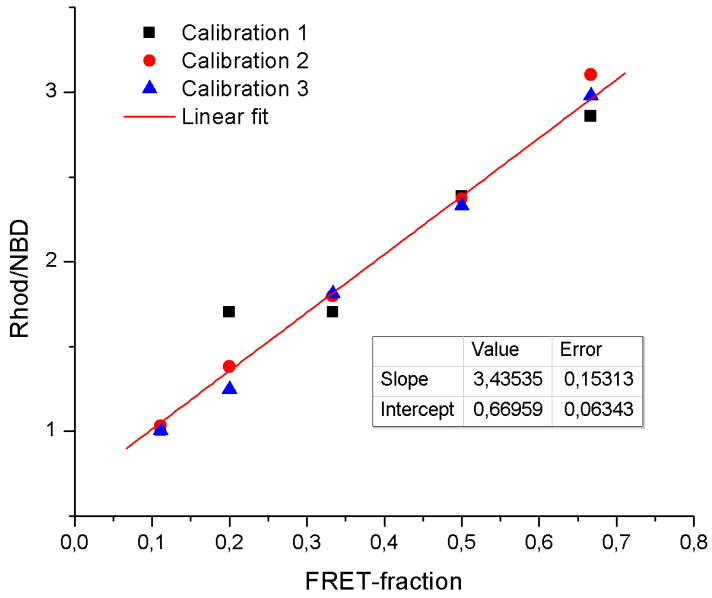

Figure 4.6: *Calibration curve for the FRET assay, obtained from three independent measurements of the same reference sample.*

4.2 Quantifications of various vesicle species

Having successfully established and calibrated the FRET assay, we now wish to use it to quantify various species of vesicles/lipid nanoparticles with different compositions and properties. Ideally, the assay can be used to quantify lipid nanoparticles of biological origin. Biological membranes consist of various types of lipids and have extreme structural complexity, such as embedded proteins, lipid rafts, and cholesterol. All of these factors could possibly affect membrane fusion.

We confirmed membrane fusion and tested the FRET assay on several species of synthetic and naturally occurring vesicles species and quantified the membrane surface area using the calibration curve established in Section 4.1. We then compared the results to alternative quantification methods.

4.2.1 Quantification of POPC vesicles containing cholesterol

An important constituent of biological membranes is cholesterol, a sterol type lipid which embeds itself amongst the phospholipids [12], affecting various structural properties of the membrane such as fluidity [32], permeability [32] and thickness [33]. Cholesterol is an essential building block in all animal cell membranes, representing up to 40 mol% [33] of animal cell plasma membranes. In particular, cholesterol is involved in phase transition of POPC into liquid ordered phase (lipid rafts) [34].

To test the compatibility of the FRET assay with cholesterol-containing vesicles and to see how a different lipid phase affects vesicle fusion, we prepared cholesterol-containing POPC vesicles in HBS, with equal molar content of POPC and cholesterol. At this cholesterol concentration the membrane is expected to be purely in liquid-ordered phase [34].

We sonicated various ratios of FRET/cholesterol vesicles to confirm vesicle fusion. In Figure 4.7 A) we see that the peak ratio lowers as concentration of drain vesicles increases, clearly indicating that the source and drain vesicles are fusing in a concentration-dependent manner.

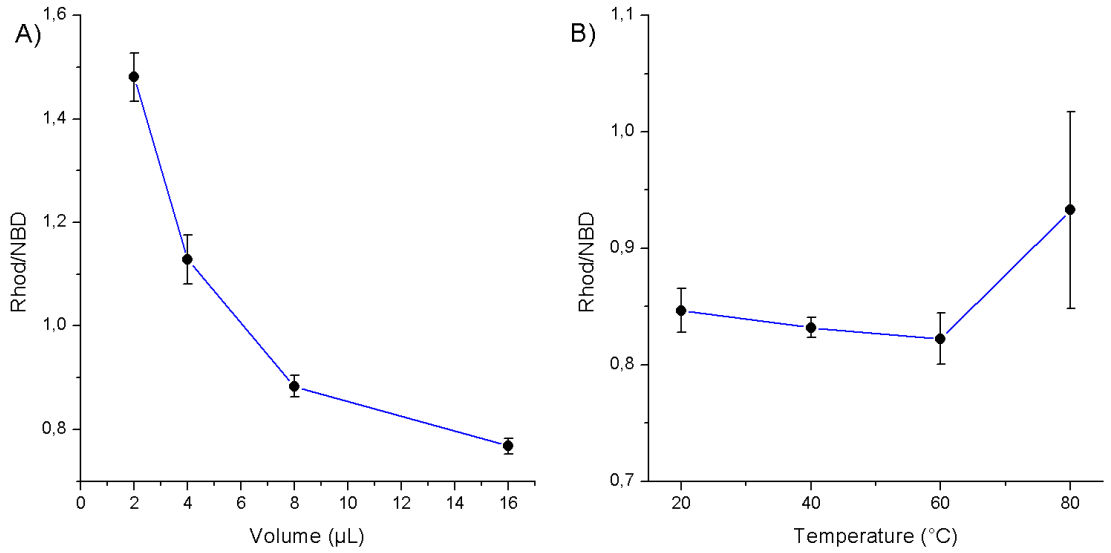

Figure 4.7: *A) FRET assay measurements of several different volumes of cholesterol-containing vesicles at 40°C. B) Temperature analysis on 8 µL cholesterol-containing vesicles. Sonication time was 20 minutes for all datapoints. Data is the average of 3 independent measurements and error bars their standard deviation.*

To determine at which conditions maximal lipid mixing is achieved, we sonicated FRET and drain vesicles at fixed ratios but different temperatures. In Figure 4.7 B) we see clear sign of vesicle fusion, and furthermore that the fusion is unaffected by sonication temperature, except possibly for 80°C, were fusion seems to be lower. We can therefore quantify the surface area of our cholesterol vesicles with the FRET assay. We selected the 2 µL measurement to use for quantification, as it falls closest to the center of the linear region of the calibration curve. Results can be seen in Table 4.3. Finally, we also characterized the vesicles with NTA and the phosphorus assay and compared the results (Table 4.3).

Table 4.3: *Numerical results for cholesterol-containing vesicles.*

FRET assay	Phosphorus assay	NTA		
SAC (nm^2/mL $\times 10^{17}$)	POPC conc. (mg/mL)	Mean diameter (nm)	Particles/mL ($\times 10^{12}$)	SAC (nm^2/mL $\times 10^{17}$)
$8,0 \pm 1,1$	$1,33 \pm 0,074$	129 ± 5	$3,69 \pm 0,16$	$2,53 \pm 0,18$

The results from the NTA size determination indicate that the mean diameter of the cholesterol-containing vesicles is similar to both the FRET and POPC vesicles. The SAC measured by the NTA is less than a third of the one measured by the FRET assay, indi-

cating that the FRET assay is more sensitive to surface area than NTA. Our comparison further reveals that both the FRET-assay and NTA have similar errors, 7,2 % and 7,1 %.

Of note is that particle concentration of the cholesterol-containing vesicles is almost twice as high as the POPC vesicles used in calibration, despite lower lipid content (see Table 4.2 for comparison value). The cause of this might be the reduction in area-per-lipid of phospholipids caused by cholesterol, which might increase their optical density, rendering them more visible in the NTA, and therefore allowing for the detection of smaller vesicles i.e. of a larger fraction of the vesicle population.

Results from the phosphorus assay indicate that the effective POPC lipid concentration was higher than the theoretical one, estimated from the lipid stock used (1 mg POPC/mL). Overall, the results indicate that the FRET assay can be used to quantify the surface area concentrations of cholesterol-embedded vesicles.

4.2.2 OMV quantification

We are interested in finding out if the assay can be used to quantify lipid nanoparticles of biological origin. Biological particles have complex membranes, with various lipid species and embedded surface proteins. In order to test the suitability of our assay for biological particles, we tested our FRET-assay on two species of OMV's extracted from Escherichia coli virus (*E. coli*), one from **w**ild-**t**ype (**WT**), the other from **hldE** mutant with truncated lipopolysaccharide on the outer membrane. The vesicle concentration is unknown.

We sonicated varying volumes of OMV's to determine whether the OMV's successfully fuse with the FRET vesicles. To determine at which conditions maximal lipid mixing is achieved, we sonicated FRET and drain vesicles at fixed ratios but different temperatures. Results can be seen in Figure 4.8. We see that for both types of OMV the peak ratio lowers as concentration of drain vesicles increases, clearly indicating that the source and drain vesicles are fusing in a concentration dependent manner. Furthermore, we see that the fusion of both OMV's is unaffected by sonication temperature; we can therefore quantify the surface area of the OMV's with the FRET assay. We chose the measurement at 40°C to use in quantification, to match the temperature of our calibration curve. Results can be seen in Table 4.4.

Table 4.4: *Numerical results for OMV's.*

	FRET assay	NTA		
	SAC (nm^2/mL $\times 10^{17}$)	Mean diameter (nm)	Particles/mL ($\times 10^{11}$)	SAC (nm^2/mL $\times 10^{16}$)
hldE	$7,22 \pm 0,85$	123 ± 4	$1,87 \pm 0,32$	$1,18 \pm 0,10$
WT	$2,40 \pm 0,22$	119 ± 5	$2,6 \pm 1,1$	$1,48 \pm 0,56$

As a next step, we characterize the OMV's with NTA and compare the results. Results can be seen in Table 4.4. The SAC measured by the NTA is less than a sixth of the value measured by the FRET assay for the hldE, and less than a sixteenth for the WT OMV'S. These results indicate that the NTA is not measuring nearly all the particles in the samples, and that the FRET assay is far more sensitive to surface area than NTA. On

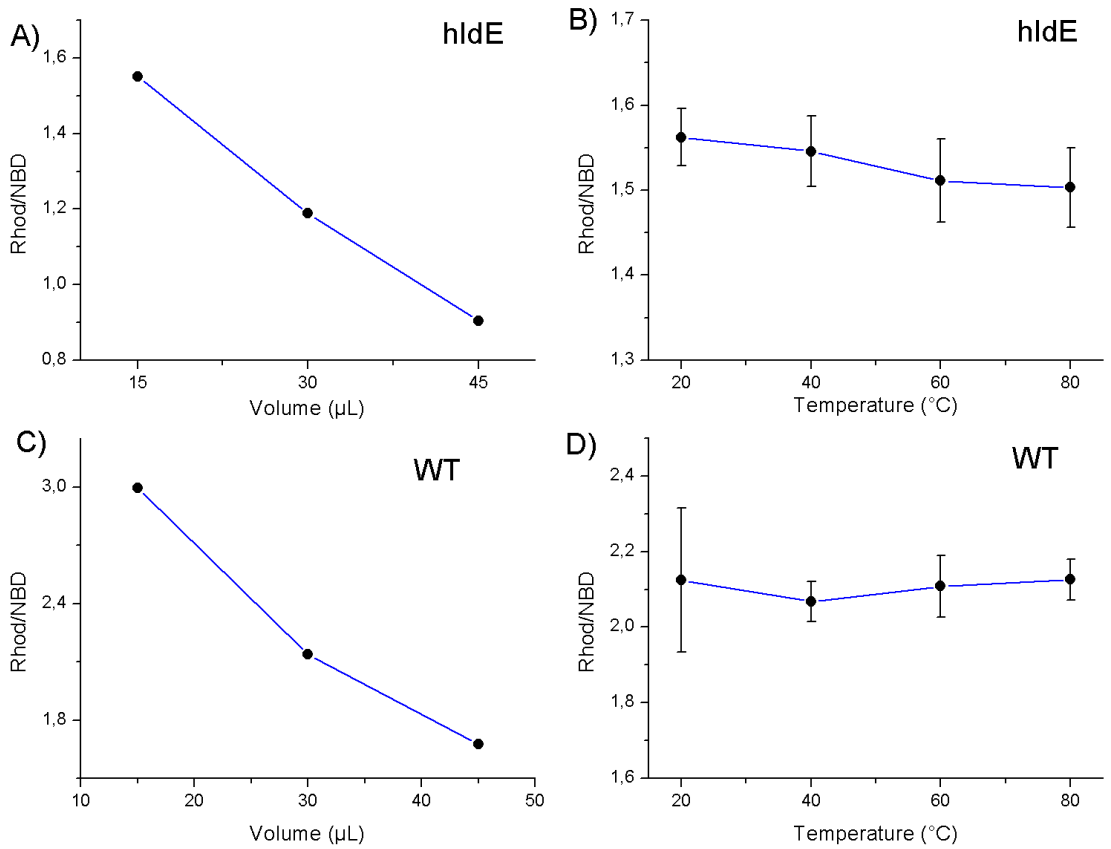

Figure 4.8: *FRET assay measurements of several different volumes of A): hldE, and C): WT OMV's at 40°C. Each datapoint is one sample. Temperature analysis of B): 20 µL hldE OMV's, and D): 30 µL WT OMV's. Each datapoint is the average of three samples, with standard deviation as error. All sonications were 20 minutes.*

the other hand, the error of the FRET assay is 12 % for the hldE, and 9,2 % for the WT OMV'S, while the error for the NTA is 8,5 % for hldE but 38 % for the WT OMV'S. This error for the WT is far larger than for all other samples; the cause is unknown. Otherwise the errors are similar.

Finally, we attempted a CBQCA protein quantification of the OMV's yielding a protein content of $1,85 \pm 0,25$ mg/mL for the hldE OMVs and $1,83 \pm 0,20$ mg/mL for the WT. Considering the total surface area determined with our assay, we can then determine the amount of protein / area of lipid membrane, yielding values of $2,56 \times 10^{-20}$ g/nm^2 and $7,6 \times 10^{-20}$ g/nm^2 respectively. These values are rather high, if one considers, for comparison, that an *E. coli* bacteria is 6 µm^2 (6×10^6 nm^2), and has a total protein mass of around 15×10^{-14} g/cell[35], yielding a protein surface density of $2,5 \times 10^{-20}$ g/nm^2, if one assumes that all proteins are distributed to the membrane only. Furthermore, it should be noted that this concentration may be an underestimation of the actual protein content as these measurement was performed outside the calibration range (supplement B). These values indicate that either the OMV's contain protein cargos, and therefore have similar protein density as the origin cells, or that there are large amounts of free proteins in the samples. The presence of free proteins in the samples was confirmed with TEM imaging performed by Madeleine Ramstedt (image not shown here).

4.2.3 Virus quantification

Another category of biological samples of interest are membrane-enveloped viruses, such as herpes-simplex virus. A quantification of their surface area would be an alternative method of quantifying the concentration of such a viral sample.

The FRET-assay was tested on inactivated herpes-simplex viral suspensions. A volume gradient was performed to confirm that vesicle fusion is taking place during sonication. The results can be seen in Figure 4.9 A). The peak ratio drops with increasing volume, indicating that the viral particles and FRET vesicles are fusing in a volume dependent manner.

Temperature analysis was performed at Chalmers by Eneas Schmidt. Results seem to indicate higher vesicle fusion for higher temperature (see Figure 4.9 B), although it's hard to draw any conclusions due to the large error bars. We decided to err on the side of caution and do quantifications at 80°C. We chose 30 µL to use in quantification.

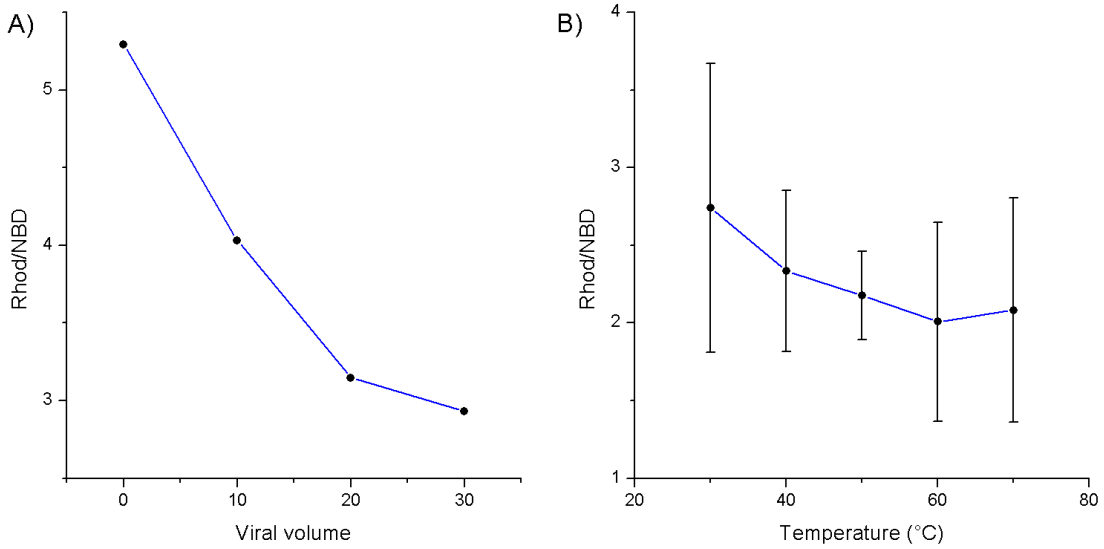

Figure 4.9: *A) FRET assay measurements of several different volumes of HSV-2 at 80°C. B) Temperature analysis for viral samples. All sonications were 20 minutes. Temperature measurements were performed at Chalmers by Eneas Schmidt.*

The viral samples were also analyzed with NTA and CBQCA protein assay kit. Results can be seen in Table 4.5. The viral particles have a mean diameter of 151 nm, larger than the particles characterized previously in this study. Correspondingly, the SAC measured by the NTA are similar to the SAC measured by the FRET assay, indicating that in this case, most of the particles are most likely detected by NTA as well.

Table 4.5: *Numerical results for viral samples.*

FRET assay	NTA			CBQCA
SAC (nm^2/mL $\times 10^{15}$)	Mean diameter (nm)	Particles/mL ($\times 10^{10}$)	SAC (nm^2/mL $\times 10^{15}$)	Protein content (mg/mL)
$8,99 \pm 0,65$	151 ± 10	$8,67 \pm 0,31$	$8,8 \pm 1,0$	$0,071 \pm 0,013$

For comparison, we also did a CBQCA protein quantification kit, to measure the total protein content of the viral sample. We measured two volumes in triplicate, 13 µL and 26 µL, resulting in protein content of $0,071 \pm 0,013$ mg/mL. Using the particle concentration from the NTA, we obtain a protein content of $8,2 \pm 1,8 \times 10^{-16}$ g/virion. This value is in relatively good agreement with the total protein content of the structurally similar HSV-1 virus which has been reported in the literature to be around $16,4 - 19,4 \times 10^{-16}$ g/virion[36].

5
Discussion

5.1 Assay performance

In this work, we have developed a FRET-based method, to quantify the total surface area of lipid membranes. A primary concern for this thesis is how the assay performs in quantifying lipid nanoparticle samples, and how the method compares to currently established methods.

5.1.1 Accuracy

When discussing the overall performance of our assay, a first question to be raised concerns its accuracy. Indeed, we need to know if the results for the SAC obtained by the FRET-assay are close to the 'true concentration value' of the sample. For instance, if the vesicle fusion is not 100 % efficient, but some amount of material remains unfused after sonication, the assay will give an underestimation of the surface area. In particular, this effect could be dependent on the type of lipids in the sample.

In order to evaluate the performance of the assay we performed quantifications of our samples with alternative established measurement methods, and compared the results to the FRET assay.

Nanoparticle tracking analysis

Our primary choice of comparison method was NTA. NTA works well as a comparison method for this project, because NTA measures size distribution, which can easily be converted to surface area concentration. We can therefore directly compare the results of our FRET assay to the results from NTA. In Table 5.1 we see the ratio between the FRET-assay results and the NTA results, along with the mean diameter measured by the NTA.

Table 5.1: *The ratio between FRET and NTA SAC measurements, along with mean diameter measured in the NTA.*

	Mean diameter (nm)	FRET-assay/NTA (SAC ratio)
Cholesterol-vesicles	129 ± 5	3,2
OMV-hldE	123 ± 4	6,1
OMV-WT	119 ± 5	16
HSV-2	151 ± 10	1,02

Our results indicate that the FRET-assay measures larger SAC than NTA for all samples except for the HSV-2 virus sample, where the results are comparable. Our hypothesis is that the observed difference may be a consequence of the limited ability of NTA of detecting the entire vesicle population due to a too low scattering signal which is determined by the particle's size and the particle's optical density. In line with the idea that some vesicles within a vesicle population may be too small to be detected by NTA, leading to an underestimation in the SAC, we see that the relative difference between the SAC detected with the FRET assay and using NTA, seems to be directly related to the mean diameter, with particles of smaller mean diameter having larger relative difference. Another factor that may be play a key role in determining NTA accuracy is the optical density of the particles. Their refractive index being close to the one of water, lipid nanoparticles are relatively transparent in aqueous solution, and therefore not easily detected by NTA. Viral particles on the other hand contain the capsid protein and the viral genetic material, rendering them optically denser than liposomes, and therefore more likely to be detected by NTA

Data from the NanoSight NTA, an alternative NTA device to the ZetaView used here (see Supplement C) further supports the idea that the ZetaView does not detect all vesicles. Indeed, using NanoSight to characterize the OMV's, which had the smallest diameter in the ZetaView measurements, we obtain significantly lower values for the mean diameters of the OMV's (102 and 88 nm for hldE and WT respectively) and accordingly higher SAC, indicating that there is a large population of small particles not detected by the ZetaView NTA and that the NanoSight NTA device might be superior in sensitivity. A particular concern regarding the accuracy of ZetaView, as compared to the NanoSight NTA measurements, is that the program does now explicitly show particles being detected. This makes it hard to optimize the measurement parameters, which is particularly crucial for measurements of small particles where the parameters need to be optimized to make sure that most particles are detected without capturing background noise. This may cause the operator to perform measurements at suboptimal parameters, vastly skewing results and further contributing to discrepancies in the results obtained in different NTA devices. This also means that it is difficult to obtain accurate comparison values of the 'true' SAC of our samples to compare with the FRET assay.

Phosphorus assay

To obtain a more direct comparison between the FRET assay and the phosphorus content, we were able to determine the SAC from the phosphorus content, based on literature values for the area-per-lipid of POPC and cholesterol in membranes. Cholesterol is known to cause a reduction in area-per-lipid in membranes, an effect known as the 'condensing effect'[32,37–39], reducing POPC area-per-lipid value of POPC down to around 0,4 - 0,5 nm^2 at 50 mol% cholesterol[32,38,39]. The area-per-lipid values vary between studies; we used values for the areas-per-lipid of POPC and cholesterol from Loura *et al.* (2013) for calculations (0,51 nm^2 for POPC, 0,26 nm^2 for cholesterol). Using these values, we obtain a SAC of $3,7 \times 10^{17}$ nm^2/mL, which is of a comparable order of magnitude to the value obtained with the FRET-assay ($8,0 \pm 1,1 \times 10^{17}$ nm^2/mL), indicating the FRET assay is obtaining reasonably accurate values for the SAC. The value obtained from the phosphorus assay should be taken with some reservation however, as there is a lack of agreement in literature on the precise values for the area-per-lipid of POPC and cholesterol. In particular, values for cholesterol range between 0,2-0,4 nm^2 between articles[37,39]. The effects of cholesterol on the area-per-lipid of POPC (the so-called condensing effect) is also dependent on the

mol

5.1.2 Assay precision

Another concern for this project is the precision of the assay which is related to the error of a quantification measurement. For SAC quantifications in the FRET-assay the standard deviation of three independent measurements of a single reference sample is used as error. For all the quantification experiments performed in this project, the average error for lipid nanoparticle quantifications was 11 %, with a standard deviation of 3 % and a maximum error of 19 % (WT-OMV's sonicated at 20°C). This indicates that the precision of our assay is consistent. Such errors are of the same magnitude than the ones reported with the NTA. In our hands, the average error for the NTA measurements we performed with the ZetaView, was 7,6 %, with standard deviation 2,3 %. (in this case, we omit the measurements on WT OMVs, which exhibited an error of 38 %) while the average error obtained with NanoSight was 26 %. In literature, we find that the error values obtained for NanoSight NTA are in the range of 5-10 %[5,14,15]; the large error values for our NanoSight measurements are therefore likely to be related to the operator's lack of experience with the device.

Coming back to our FRET assay, there are probably some aspects of the sonication procedure that could be refined and/or optimized to reduce the error. For instance, we discovered during the course of this project that the water level in the sonicator needs to be around half full, and the water degassed before measurements, otherwise results will be wildly inconsistent. We also believe that the sonicator's vibrational energy is not homogeneous, which can cause samples to be unevenly sonicated. To address this we attempted to place the samples in visible vibrational hotspots in the sonicator (see Figure 3.1, Section 3.6) and to rotate the sample during sonications.

Since pipetting is a common source of error, the volume of sample used also influences precision. If smaller volumes are used, the precision of the pipettes is reduced, increasing total error. An example of this effect can be seen in the calibration curve, for higher FRET-fraction values, where the errors are noticeably larger than for lower values, corresponding to the lower volumes of POPC vesicles used (we pipetted down to 0,5 µL of POPC). We mixed large volumes of sample and aliquoted down to the 60 µL sample size to minimize this error, but improvements can possibly be made with improved pipetting techniques.

A final source of error may be some variance in the intensity measurements; scanning the same sample multiple times will give varying intensities. A closer look at 3 scans run over the same sample indicates that this variance is small compared to the other two factors mentioned: In such a case, the errors are in the order of 1-2 %.

5.1.3 Limit of detection

Finally, we are interested in the limit of detection of our assay, i.e. the minimal amount of material that can be detected, as many samples of potential interest for quantification can have very low concentrations. This could be the case, for example, in the context of quantifying lipid vesicles directly from a biological fluid or from a cell supernatant, without purification and concentration step[3,8,9].

The lowest concentration measured in this project was the wild-type OMV's, with a SAC of 2,40 nm^2/mL. Based on the extended calibration curve (Figure 4.5, Section 4.1.4), we can estimate the lowest SAC of lipid nanoparticles that can be quantified using our current assay protocol. Based on the lower end of the calibration curve (i.e. higher values

for FRET-fraction), we see that the calibration curve is linear up to FRET-fractions of 0,8. This represents the minimum amount of vesicle surface area that can be accurately quantified by the assay.

Our current experimental protocol for the FRET-assay uses volume of 60 µL for quantifications, of which 2 µL are FRET vesicles. The total surface area of 2 µL 1 mg/mL FRET vesicles is $4,95 \times 10^{14}$ nm^2. A FRET-fraction of 0,8 then corresponds to

$$0,8 = \frac{A_{FRET}}{A + A_{FRET}} = \frac{4,95 \times 10^{14} \text{ nm}^2}{A + 4,95 \times 10^{14} \text{ nm}^2}$$

$$\rightarrow A = 1,24 \times 10^{14} \text{ nm}^2$$

which, assuming the sample's total volume is 58 µL, gives a surface area concentration of:

$$\text{SAC} = \frac{1,24 \times 10^{14} \text{ nm}^2}{58 \ \mu\text{L}} = 2,13 \times 10^{15} \ \frac{\text{nm}^2}{\text{mL}}$$

For comparison, assuming a homogeneous solution of 100 nm particles, this would correspond to $6,8 \times 10^{10}$ particles/mL, or a total of $3,9 \times 10^9$ particles required to perform a quantification measurement. To our knowledge, neither the size nor size distribution (i.e. heterogeneity) of the particles matters for the FRET-assay, only the total surface area.

This limit-of-detection value holds for the composition of FRET vesicles used in this project. However, modifications to the assay protocols may be able to bring this estimate even lower. For instance, we could also use a lower concentration of FRET vesicles, requiring less material to detect peak ratio changes. This method is probably the simplest to implement. The lower limit would then be dependent on the sensitivity of the spectrofluorometer used for measurements.

Other possible ways to lower the detection limit may be to increase the total volume of sample sonicated, change the fluorophore content, or use a different fluorophore pair. These parameters would need to be analyzed better before any conclusions can be made.

Comparing with the ZetaView NTA

The ZetaView manual states that the limit of detection for the device is 10^5 particles/mL, and minimum particle size 10 nm diameter for strongly reflective metal nanoparticles. Vesicles are not very reflective, so their detection limit will be substantially higher. In literature, we find references of operational concentration of ZetaView for vesicle quantification to be around 10^7 – 10^8 particles/mL, although concentrations were believed to be underestimated, due to large populations of small vesicles not being detected [40,41]. Values for NanoSight NTA are found to be around 10^8 – 10^9 particles/mL [5,13,15]. Regardless of concentration used, NTA (both ZetaView and NanoSight) requires 1 mL volume of sample to perform measurement. This means NTA requires in total around 10^7 – 10^8 visible particles to be able to perform measurements which is 10 times less that with our FRET assay.

The concern relating to the NTA detection of smaller vesicles (discussed in Section 5.1.1) is relevant here as well. The detection limit of NTA must be discussed in relation to the size of the particles being measured. If the particles are smaller than the NTA can adequately handle, it is difficult to define what the detection limit is for these particles, and NTA may not be suited to accurately characterize them.

5.2 Theoretical model of FRET in membranes

The behavior of our calibration curve (Figure 4.5, Section 4.1.4) warrants a closer look. We see that the curve levels off for lower values of FRET-fraction, and sharply rises for higher values. A more detailed knowledge of the theoretical aspects of this curve might help with further developments of the assay, such as lowering detection limit or increasing sensitivity. The relation between the peak ratio (Rhod/NBD) and the surface area fraction of the FRET vesicles is not trivial, and should therefore be considered from an analytical perspective. The most obvious way to do this is to relate the two to the FRET efficiency E. The value of the E is most often measured using the relation [21,42]

$$E = 1 - \frac{F_D}{F_{D0}}$$

where F_D is the fluorescence intensity of the donor fluorophore in the presence of an acceptor and F_{D0} is the fluorescence of the donor in the absence of an acceptor. The latter is commonly measured either by photobleaching the acceptor fluorophores [23,42,43] or by adding a detergent to separate the fluorophores [44].

In this project, we have utilized ratiometric FRET, based on the intensity ratio between the donor and acceptor fluorophores [42]. The advantage of ratiometric FRET is higher signal-to-noise ratio (since both intensities are used) [42,45], and it is simpler than conventional FRET as it doesn't require spectral correction (due to wavelength dependence of instruments) or measurements of fluorophore lifetime [46]. The biggest flaw with ratiometric FRET is that it can't be used to measure the FRET efficiency directly [42]. Several correction factors must be determined in order to evaluate the FRET efficiency from ratiometric measurements.

Using a model presented by McCann et al. (2010) to correlate the FRET efficiency E to the donor and acceptor intensities I_D and I_A, we can write the FRET-efficiency as

$$E = \frac{I_A - \beta I_D}{I_A - \beta I_D + \gamma I_D}$$

where β corrects for donor leakage into the acceptor intensity, and γ accounts for the differences in quantum yields and detector sensitivity of the two fluorophores [43]. From this equation we can derive a relation between the efficiency E and the intensity ratio $I = I_A/I_D$:

$$E = \frac{I_A - \beta I_D}{I_A - \beta I_D + \gamma I_D} = \frac{I - \beta}{I - \beta + \gamma}$$

$$\rightarrow \frac{1}{E} = 1 + \frac{\gamma}{I - \beta}$$

$$\rightarrow \frac{1 - E}{E} = \frac{\gamma}{I - \beta}$$

$$\rightarrow I = \beta + \frac{\gamma E}{1 - E} \tag{5.1}$$

Now we must consider how the distance r between donor and acceptor fluorophores, and the FRET surface area fraction F, relate. This presents some challenges, as our system contains multiple donors and acceptors freely diffusing in a spherical membrane, both on the inner and outer layers. This is a highly complex system, which is difficult to analyze analytically. We will start by making a simplified model, and see where it gets us.
Assume the following:

- Fluorophores don't interact between the inner and outer layers of the liposomes.
- Each donor fluorophore interacts only with a single nearest neighbor acceptor (and vice versa).
- We can ignore the effects of the spherical shape of the liposomes on the distance between two nearest neighbor fluorophores.
- Fluorophores are evenly spread on the surface and have a fixed position.

Now consider a FRET vesicle made up of $2N$ lipids, with a fluorophore content of 2 mol% (equal parts donor and acceptor). Since the vesicle is a bilayer there are N lipids in the outer layer and N lipids in the inner layer. Let's now assume that this FRET vesicle fuses with a drain vesicle made of the same lipid species, with $2M$ lipids. The outer surface area A of this newly fused vesicle is then

$$A = (N + M) \cdot a$$

where a is the area-per-lipid of the lipid species. For simplicity, we assume that the fluorophores have the same area-per-lipid value, a reasonable assumption since the fluorophore is attached to the head group, and the lipid species is the same. Then, the area occupied by each fluorophore (a_f) is

$$a_f = \frac{A}{0,02 \cdot N} = \frac{50(N+M)a}{N} = \frac{50(N+M)a}{N} = \frac{50a}{F}$$

where F is the surface area fraction of FRET-vesicles. For simplicity's sake we assume that the area occupied by the fluorophores is square. Then the distance between two nearest fluorophores is

$$r = \sqrt{a_f} = \sqrt{\frac{50a}{F}}$$

Inserting our expression for the distance r into the expression for the FRET efficiency, we get

$$E = \frac{1}{1 + (\frac{r}{R_0})^6} = \frac{1}{1 + (\frac{\sqrt{\frac{50a}{F}}}{R_0})^6} = \frac{1}{1 + (\frac{50a}{FR_0^2})^3} \tag{5.2}$$

We see that equations 5.1 and 5.2 correlate both the intensity ratio I and the FRET-fraction F to the FRET efficiency E. Combining the equations we get

$$I = \beta + \frac{\gamma \frac{1}{1+\alpha^3}}{1 - \frac{1}{1+\alpha^3}} = \beta + \frac{\gamma}{1 + \alpha^3 - 1} = \beta + \frac{\gamma}{\alpha^3}$$

$$\rightarrow I = \beta + \frac{\gamma}{(\frac{50a}{FR_0^2})^3}$$

$$\rightarrow I = \frac{\gamma R_0^6}{50^3 a^3} F^3 + \beta \tag{5.3}$$

We see that the intensity ratio should be correlated to the FRET-fraction cubed. Although this model is based on many simplifications, it serves as a viable starting point for modelling the calibration curve behavior. Results can be seen in Figure 5.1.

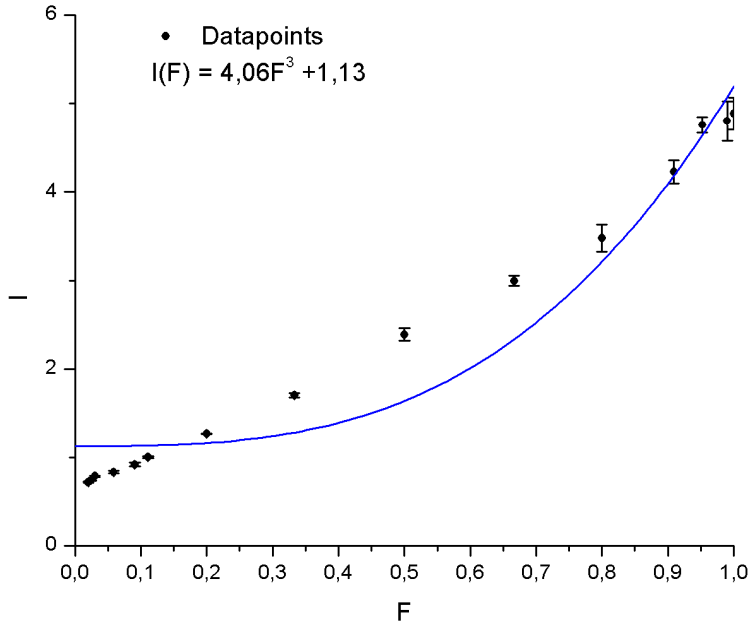

Figure 5.1: *Theoretical model of our extended calibration curve.*

As we can see, the model is not a good fit for the observed data.

We tested a more general principle of this model. Retaining the assumption that I is correlated to the FRET-fraction cubed, we did a full cubic fit. Results can be seen Figure 5.2

Based on the model in Figure 5.2, we see that the theoretical model is a reasonable fit for the data obtained in this thesis. Of the assumptions we made to simplify our model, the assumption that each donor acts with a single donor (and vice versa) is probably the most questionable assumption. Indeed, if an excited donor is in close proximity to several acceptors, the probability of FRET to occur increases significantly. This has been analyzed to some extent by Berney & Danuser (2003), both in physical models and by simulations, but their analysis assumes that the distance between fluorophores is fixed [47]. To our knowledge, no detailed analysis of multiple donors and acceptors freely diffusing in membranes has been performed. Alternatively, determination of efficiency could be skipped completely and a model relating the intensity ratio to the fluorophore concentration could be developed.

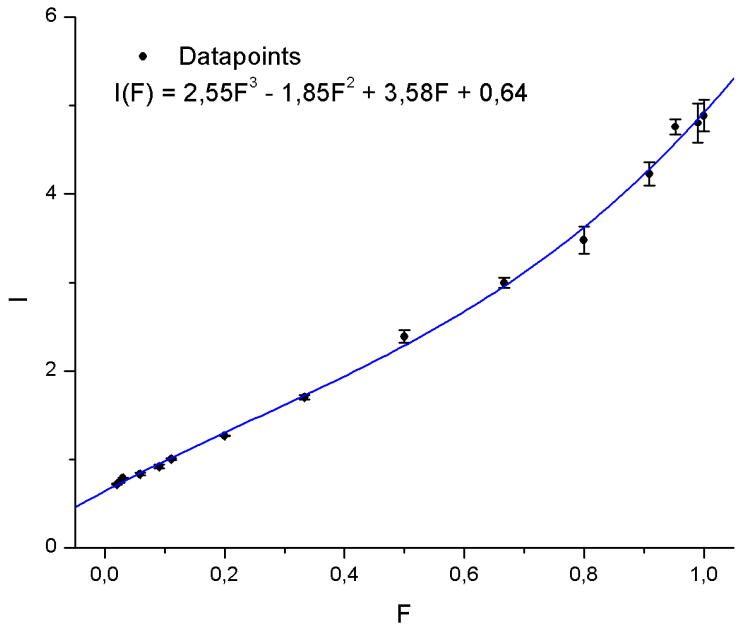

Figure 5.2: *Theoretical model fitted to the datapoints of the extended calibration curve, assuming full cubic relation.*

5.3 Conclusions

Based on the work presented in this thesis, we conclude that the assay can serve as a useful measurement technique to determine vesicle concentrations. The method is demonstrated to be reliable and precise, and can be used to quantify various types of lipid nanoparticles of both biological and synthetic origin. Our method also demonstrates some advantages compared to alternative methods, such as being capable of detecting smaller particles than NTA, and being unaffected by byproducts in the samples (free proteins in the OMV and virus samples), which represents a considerable advantage for the study of biological lipid nanoparticle samples.

The primary concern is the accuracy of the assay; our results deviate from values obtained with alternative measurement method (NTA and phosphorus assay), and although we've presented some theories as to what causes this, further analysis is required to ensure the veracity of these theories. There is also some concern over the limit of detection of the method. The assay, in its current form, requires more material for quantification than the alternative methods presented here, but far less volume. We have presented some ideas for improvements, which would need to be tested in order to optimize the assay. The assay also needs to be tested at different lab, with different devices, to ensure reproducibility of our results.

References

[1] Allen, T. M. and Cullis, P. R. (2013) Liposomal drug delivery systems: From concept to clinical applications. *Advanced Drug Delivery Reviews,* **65**(1), 36–48.

[2] Rupert, D. L. M., Claudio, V., Lasser, C., and Bally, M. (2017) Methods for the physical characterization and quantification of extracellular vesicles in biological samples. *Biochimica Et Biophysica Acta-General Subjects,* **1861**(1), 3164–3179.

[3] van der Pol, E., Boing, A. N., Harrison, P., Sturk, A., and Nieuwland, R. (2012) Classification, Functions, and Clinical Relevance of Extracellular Vesicles. *Pharmacological Reviews,* **64**(3), 676–705.

[4] van der Pol, E., Coumans, F. A. W., Grootemaat, A. E., Gardiner, C., Sargent, I. L., Harrison, P., Sturk, A., van Leeuwen, T. G., and Nieuwland, R. (2014) Particle size distribution of exosomes and microvesicles determined by transmission electron microscopy, flow cytometry, nanoparticle tracking analysis, and resistive pulse sensing. *Journal of Thrombosis and Haemostasis,* **12**(7), 1182–1192.

[5] Gardiner, C., Ferreira, Y. J., Dragovic, R. A., Redman, C. W., and Sargent, I. L. (2013) Extracellular vesicle sizing and enumeration by nanoparticle tracking analysis. *J Extracell Vesicles,* **2**.

[6] Hole, P., Sillence, K., Hannell, C., Maguire, C. M., Roesslein, M., Suarez, G., Capracotta, S., Magdolenova, Z., Horev-Azaria, L., Dybowska, A., Cooke, L., Haase, A., Contal, S., Mano, S., Vennemann, A., Sauvain, J. J., Staunton, K. C., Anguissola, S., Luch, A., Dusinska, M., Korenstein, R., Gutleb, A. C., Wiemann, M., Prina-Mello, A., Riediker, M., and Wick, P. (2013) Interlaboratory comparison of size measurements on nanoparticles using nanoparticle tracking analysis (NTA). *Journal of Nanoparticle Research,* **15**(12).

[7] Sercombe, L., Veerati, T., Moheimani, F., Wu, S. Y., Sood, A. K., and Hua, S. (2015) Advances and Challenges of Liposome Assisted Drug Delivery. *Frontiers in Pharmacology,* **6**.

[8] Raposo, G. and Stoorvogel, W. (2013) Extracellular vesicles: Exosomes, microvesicles, and friends. *Journal of Cell Biology,* **200**(4), 373–383.

[9] van Niel, G., D'Angelo, G., and Raposo, G. (2018) Shedding light on the cell biology of extracellular vesicles. *Nature Reviews Molecular Cell Biology,* **19**(4), 213–228.

[10] Schwechheimer, C. and Kuehn, M. J. (2015) Outer-membrane vesicles from Gram-negative bacteria: biogenesis and functions. *Nature Reviews Microbiology,* **13**(10), 605–619.

[11] Buchmann, J. P. and Holmes, E. C. (2015) Cell Walls and the Convergent Evolution of the Viral Envelope. *Microbiology and Molecular Biology Reviews,* **79**(4), 403–418.

[12] Lodish, H., Berk, A., Kaiser, C. A., Krieger, M., Bretscher, A., Ploegh, H., Amon, A., and Martin, K. C. (2016) Molecular cell biology, W.H. Freeman-Macmillan Learning, New York eighth edition. edition.

[13] Dragovic, R. A., Gardiner, C., Brooks, A. S., Tannetta, D. S., Ferguson, D. J. P., Hole, P., Carr, B., Redman, C. W. G., Harris, A. L., Dobson, P. J., Harrison, P., and Sargent, I. L. (2011) Sizing and phenotyping of cellular vesicles using Nanoparticle Tracking Analysis. *Nanomedicine-Nanotechnology Biology and Medicine,* **7**(6), 780–788.

[14] Filipe, V., Hawe, A., and Jiskoot, W. (2010) Critical Evaluation of Nanoparticle Tracking Analysis (NTA) by NanoSight for the Measurement of Nanoparticles and Protein Aggregates. *Pharmaceutical Research,* **27**(5), 796–810.

[15] Vestad, B., Llorente, A., Neurauter, A., Phuyal, S., Kierulf, B., Kierulf, P., Skotland, T., Sandvig, K., Haug, K. B. F., and Ovstebo, R. (2017) Size and concentration analyses of extracellular vesicles by nanoparticle tracking analysis: a variation study. *Journal of Extracellular Vesicles,* **6**(1), 1–11.

[16] Kramberger, P., Ciringer, M., Strancar, A., and Peterka, M. (2012) Evaluation of nanoparticle tracking analysis for total virus particle determination. *Virology Journal,* **9**.

[17] Murphy, J. and Riley, J. P. (1958) A Single-Solution Method for the Determination of Soluble Phosphate in Sea Water. *Journal of the Marine Biological Association of the United Kingdom,* **37**(1), 9–14.

[18] Murphy, J. and Riley, J. P. (1962) A Modified Single Solution Method for Determination of Phosphate in Natural Waters. *Analytica Chimica Acta,* **26**(1), 31–36.

[19] Paraskova, J. V., Rydin, E., and Sjoberg, P. J. R. (2013) Extraction and quantification of phosphorus derived from DNA and lipids in environmental samples. *Talanta,* **115**, 336–341.

[20] You, W. W., Haugland, R. P., Ryan, D. K., and Haugland, N. P. (1997) 3-(4-carboxybenzoyl)quinoline-2-carboxaldehyde, a reagent with broad dynamic range for the assay of proteins and lipoproteins in solution. *Analytical Biochemistry,* **244**(2), 277–282.

[21] Lakowicz, J. R. (2006) Principles of fluorescence spectroscopy, Springer, New York 3rd edition.

[22] Stryer, L. and Haugland, R. P. (1967) Energy Transfer - a Spectroscopic Ruler. *Proceedings of the National Academy of Sciences of the United States of America,* **58**(2), 719–726.

[23] Ma, L. L., Yang, F., and Zheng, J. (2014) Application of fluorescence resonance energy transfer in protein studies. *Journal of Molecular Structure,* **1077**, 87–100.

[24] Truong, K. and Ikura, M. (2001) The use of FRET imaging microscopy to detect protein-protein interactions and protein conformational changes in vivo. *Current Opinion in Structural Biology,* **11**(5), 573–578.

[25] Shi, J. Y., Tian, F., Lyu, J., and Yang, M. (2015) Nanoparticle based fluorescence resonance energy transfer (FRET) for biosensing applications. *Journal of Materials Chemistry B,* **3**(35), 6989–7005.

[26] Vanderwerf, P. and Ullman, E. F. (1980) Monitoring of phospholipid vesicle fusion by fluorescence energy transfer between membrane-bound dye labels. *Biochim Biophys Acta,* **596**(2), 302–14.

[27] Struck, D. K., Hoekstra, D., and Pagano, R. E. (1981) Use of Resonance Energy-Transfer to Monitor Membrane-Fusion. *Biochemistry,* **20**(14), 4093–4099.

[28] Pace, H., Simonsson Nystrom, L., Gunnarsson, A., Eck, E., Monson, C., Geschwindner, S., Snijder, A., and Hook, F. (2015) Preserved transmembrane protein mobility in polymer-supported lipid bilayers derived from cell membranes. *Anal Chem,* **87**(18), 9194–203.

[29] Peerboom, N., Schmidt, E., Trybala, E., Block, S., Bergstrom, T., Pace, H. P., and Bally, M. (2018) Cell Membrane Derived Platform To Study Virus Binding Kinetics and Diffusion with Single Particle Sensitivity. *ACS Infect Dis,* **4**(6), 944–953.

[30] Kucerka, N., Nieh, M. P., and Katsaras, J. (2011) Fluid phase lipid areas and bilayer thicknesses of commonly used phosphatidylcholines as a function of temperature. *Biochimica Et Biophysica Acta-Biomembranes,* **1808**(11), 2761–2771.

[31] Berger, N., Sachse, A., Bender, J., Schubert, R., and Brandl, M. (2001) Filter extrusion of liposomes using different devices: comparison of liposome size, encapsulation efficiency, and process characteristics. *International Journal of Pharmaceutics,* **223**(1-2), 55–68.

[32] Worthman, L. A. D., Nag, K., Davis, P. J., and Keough, K. M. W. (1997) Cholesterol in condensed and fluid phosphatidylcholine monolayers studied by epifluorescence microscopy. *Biophysical Journal,* **72**(6), 2569–2580.

[33] Simons, K. and Sampaio, J. L. (2011) Membrane Organization and Lipid Rafts. *Cold Spring Harbor Perspectives in Biology,* **3**(10).

[34] de Almeida, R. F. M., Fedorov, A., and Prieto, M. (2003) Sphingomyelin/phosphatidylcholine/cholesterol phase diagram: Boundaries and composition of lipid rafts. *Biophysical Journal,* **85**(4), 2406–2416.

[35] Phillips, R. (2013) Physical biology of the cell, Garland Science, London New York, NY second edition / edition.

[36] Heine, J. W., Honess, R. W., Cassai, E., and Roizman, B. (1974) Proteins Specified by Herpes-Simplex Virus .2. Virion Polypeptides of Type 1 Strains. *Journal of Virology,* **14**(3), 640–651.

[37] McConnell, H. M. and Radhakrishnan, A. (2003) Condensed complexes of cholesterol and phospholipids. *Biochimica Et Biophysica Acta-Biomembranes,* **1610**(2), 159–173.

[38] Leftin, A., Molugu, T. R., Job, C., Beyer, K., and Brown, M. F. (2014) Area per Lipid and Cholesterol Interactions in Membranes from Separated Local-Field C-13 NMR Spectroscopy. *Biophysical Journal,* **107**(10), 2274–2286.

[39] Loura, L. M. S., do Canto, A. M. T. M., and Martins, J. (2013) Sensing hydration and behavior of pyrene in POPC and POPC/cholesterol bilayers: A molecular dynamics study. *Biochimica Et Biophysica Acta-Biomembranes,* **1828**(3), 1094–1101.

[40] Tian, Y., Ma, L., Gong, M. F., Su, G. Q., Zhu, S. B., Zhang, W. Q., Wang, S., Li, Z. B., Chen, C. X., Li, L. H., Wu, L. N., and Yan, X. M. (2018) Protein Profiling and Sizing of Extracellular Vesicles from Colorectal Cancer Patients via Flow Cytometry. *Acs Nano,* **12**(1), 671–680.

[41] Castoldi, M., Kordes, C., Sawitza, I., and Haussinger, D. (2016) Isolation and characterization of vesicular and non-vesicular microRNAs circulating in sera of partially hepatectomized rats. *Scientific Reports,* **6**.

[42] Bajar, B. T., Wang, E. S., Zhang, S., Lin, M. Z., and Chu, J. (2016) A Guide to Fluorescent Protein FRET Pairs. *Sensors,* **16**(9).

[43] McCann, J. J., Choi, U. B., Zheng, L. Q., Weninger, K., and Bowen, M. E. (2010) Optimizing Methods to Recover Absolute FRET Efficiency from Immobilized Single Molecules. *Biophysical Journal,* **99**(3), 961–970.

[44] Wolf, D. E., Winiski, A. P., Ting, A. E., Bocian, K. M., and Pagano, R. E. (1992) Determination of the Transbilayer Distribution of Fluorescent Lipid Analogs by Nonradiative Fluorescence Resonance Energy-Transfer. *Biochemistry,* **31**(11), 2865–2873.

[45] Holden, M. (2016) A Linear Measure of Forster Resonant Energy Transfer (Fret) Efficiency Incorporating a Shot Noise Uncertainty Model for Fluorescence Microscopy Intensity Images. *2016 Ieee 13th International Symposium on Biomedical Imaging (Isbi),* pp. 672–675.

[46] Tadross, M. R., Park, S. A., Veeramani, B., and Yue, D. T. (2009) Robust approaches to quantitative ratiometric FRET imaging of CFP/YFP fluorophores under confocal microscopy. *Journal of Microscopy-Oxford,* **233**(1), 192–204.

[47] Berney, C. and Danuser, G. (2003) FRET or no FRET: A quantitative comparison. *Biophysical Journal,* **84**(6), 3992–4010.

A

Calculations

A.1 Converting lipid concentration to surface area

In order to calibrate the assay with respect to surface area, we must convert the lipid concentration (mg/mL) to surface area concentration (SAC, nm^2/mL). This can be done by using literature values for the area-per-lipid of the lipid species in question. Given a lipid solution with concentration C, we can calculate the number of lipids per mL N:

$$N = \frac{C}{M} \cdot N_A$$

Where M is the molecular weight of the lipid species, and N_A is Avogadro's constant. Knowing the area-per-lipid a_l, we can then determine S, the surface area concentration:

$$S = \frac{1}{2} \cdot N \cdot a_l$$

We divide by two since we are working with bilayers and we assume both layer have the same radius.

To take a practical example, we'll show the calculation of the SAC of 1 mg/mL FRET vesicles. Our FRET vesicles have a molecular weight of $M = 767,2$ g/mol (marginally higher than for pure POPC, due to the fluorophores). The number of lipids per mL is

$$N = \frac{1 \text{ mg/mL}}{767,2 \text{ g/mol}} \cdot 6,022 \times 10^{23} \ \frac{\text{lipids}}{\text{mol}} = 7,85 \times 10^{17} \ \frac{\text{lipids}}{\text{mol}}$$

The SAC is then

$$S = \frac{1}{2} \cdot 7,85 \times 10^{17} \ \frac{\text{lipids}}{\text{mol}} \cdot 0,63 \ \frac{\text{nm}^2}{\text{lipid}} = 2,47 \times 10^{17} \ \frac{\text{nm}^2}{\text{mL}}$$

A.2 Calculating surface area concentration from calibration curve

Here we'll demonstrate how we determine a sample's SAC from a FRET-assay measurement. Based on the calibration curve, the FRET-assay relates the intensity peak ratio I to the FRET-fraction F as

$$I = aF + b$$

where F is the FRET vesicle surface area fraction (referred to as 'FRET-fraction' in text), given by

$$F = \frac{A_{FRET}}{A_{FRET} + A_{sample}}$$

where A_{FRET} and A_{sample} are the surface areas of the FRET vesicles and the sample respectively. We know the concentration of our FRET-vesicles, so we now their surface area.
We measure a volume V of a lipid nanoparticle sample and measure a peak ratio I. Then, we have

$$I = a\frac{A_{FRET}}{A_{FRET} + A_{sample}} + b$$

We can then determine the surface area of the sample as

$$A_{sample} = \frac{aA_{FRET}}{I - b} - A_{FRET}$$

The surface area concentration S is then simply

$$S = \frac{A_{sample}}{V}$$

B

CBQCA protein assay kit calibration curve

To determine the total protein content of our biological particles, we use a commercially available CBQCA protein assay kit. The assay is calibrated using bovine serum albumin. A calibration curve was made for this assay (Figure B1).

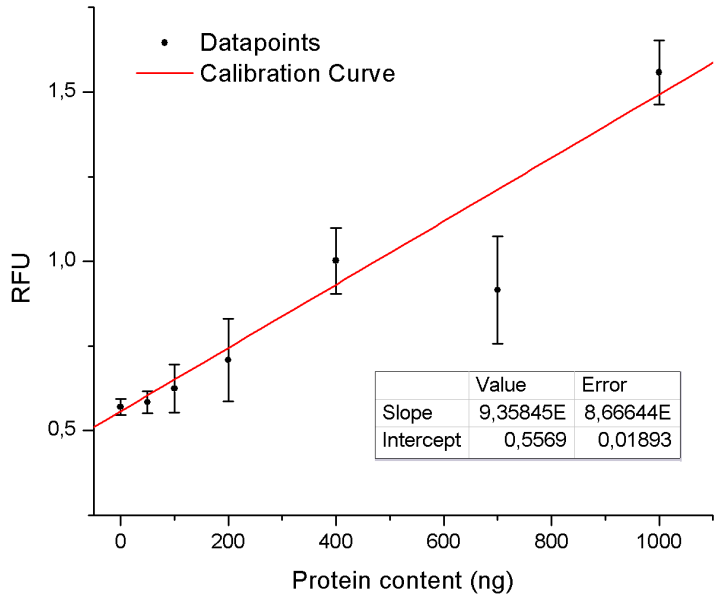

Figure B1: *Calibration curve for the CBQCA protein assay kit. Data obtained using bovine serum albumin. Each datapoint is the average of three samples, with standard deviations as errors.*

The calibration curve is capable of detecting protein content up to 1 µg. The manual for the assay indicates that the kit can be extended to protein content up to 150 µg.

C

NTA measurements performed with NanoSight device

To obtain comparison values for reference, we also ran NTA measurements on our samples (all except the viral sample, since they are more difficult to transport) using a NanoSight LM10 NTA device at the Department of Physics at Chalmers University of Technology. The primary advantage of the NanoSight NTA over ZetaView is that the operator can visually inspect the quality of particle detection and tracking, allowing the user to verify visually the parameters used for measurements.

To carry out a measurement, samples were diluted such that between 40-100 particles are visible. Measurement parameters are set after visual inspection of the acquired video data. Results of measurements can be seen in Table C1. In Tables C2 and C3 we see comparisons between the ZetaView and the NanoSight LM10.

Table C1: *Numerical data from the NanoSight LM10 device at Chalmers University. Lipid concentrations are estimated from the size distribution data.*

Sample and dilution	Mean diameter (nm)	Particles/mL ($\times 10^{12}$)	SAC (nm^2/mL $\times 10^{17}$)	Lipid concentration mg/mL
FRET vesicles (x10000)	151 ± 5	$4,66 \pm 0,44$	$4,0 \pm 1,5$	$1,61 \pm 0,60$
POPC vesicles (x10000)	143 ± 2	$8,70 \pm 0,56$	$6,24 \pm 0,88$	$2,39 \pm 0,34$
Chol vesicles (x10000)	156 ± 2	$8,62 \pm 0,42$	$7,5 \pm 1,6$	$3,02 \pm 0,63$
hldE OMV's (x1000)	102 ± 4	$0,459 \pm 0,013$	$0,186 \pm 0,064$	$0,074 \pm 0,026$
WT OMV's (x66,7)	88 ± 2	$0,0552 \pm 0,0016$	$0,0160 \pm 0,0044$	$0,0064 \pm 0,0018$

Table C2: *Comparison of numerical data between the ZetaView PMX 110 and NanoSight LM10.*

	Mean diameter (nm)		Particles/mL ($\times 10^{12}$)	
	ZetaView	NanoSight	ZetaView	NanoSight
FRET vesicles	131 ± 2	151 ± 5	$0,913 \pm 0,074$	$4,66 \pm 0,44$
POPC vesicles	124 ± 1	143 ± 2	$1,986 \pm 0,012$	$8,70 \pm 0,56$
Chol vesicles	129 ± 5	156 ± 2	$3,69 \pm 0,16$	$8,62 \pm 0,42$
hldE OMV's	123 ± 4	102 ± 4	$0,187 \pm 0,032$	$0,459 \pm 0,013$
WT OMV's	119 ± 5	88 ± 2	$0,026 \pm 0,011$	$0,0552 \pm 0,0016$

Table C3: *Comparison between the SAC obtained from the ZetaView PMX 110 and NanoSight LM10 devices.*

	SAC (nm^2/mL $\times 10^{17}$)	
	ZetaView	NanoSight
FRET vesicles	$0,655 \pm 0,042$	$4,0 \pm 1,5$
POPC vesicles	$1,265 \pm 0,061$	$6,24 \pm 0,88$
Chol vesicles	$2,53 \pm 0,18$	$7,5 \pm 1,6$
hldE OMV's	$0,118 \pm 0,010$	$0,186 \pm 0,064$
WT OMV's	$0,0148 \pm 0,0056$	$0,0160 \pm 0,0044$

We also tested the POPC vesicles at another NanoSight device, NS300, located at Umeå university. Comparison of size distributions can be seen in Figure C1. Comparison between numerical results of the three NTA devices can be seen in Table C4.

Table C4: *Mean diameters, particle concentrations and lipid concentrations of our POPC vesicles from three different NTA devices.*

	NanoSight LM10	NanoSight NS300	ZetaView PMX 110
Mean diameter (nm)	143 ± 2	141 ± 1	124 ± 1
Particles/mL ($\times 10^{12}$)	$8,70 \pm 0,56$	$2,19 \pm 0,31$	$1,987 \pm 0,015$
SAC (nm^2/mL $\times 10^{17}$)	$6,24 \pm 0,88$	$1,44 \pm 0,14$	$1,265 \pm 0,061$

As can be seen in Table C4, there is a considerable difference in results based on which

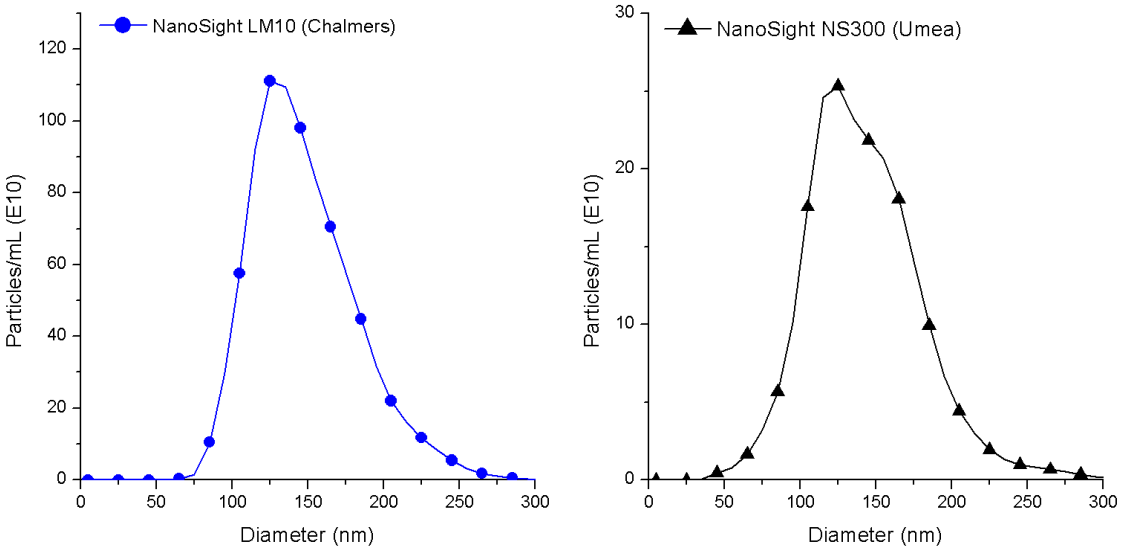

Figure C1: *Size distribution for two different NanoSight NTA devices.*

device is used. The NanoSight LM10 at Chalmers seems to be most sensitive, although the results indicate very high lipid content, higher than the phosphorus assay. Mean diameter is consistent between the NanoSight devices, but considerably lower in the ZetaView.